PHYSICAL REVIEW B VOLUME 45, NUMBER 19 15 MAY 1992-I

Inter-edge-state scattering and nonlinear effects in a two-dimensional electron gas at high magnetic fields

S. Komiyama, H. Hirai, M. Ohsawa, and Y. Matsuda
Department of Pure and Applied Sciences, University of Tokyo, Komaba 3-8-1, Meguro-ku, Tokyo, Japan

S. Sasa and T. Fujii
Semiconductor Materials Laboratory, Fujitsu Laboratories, Limited, Ono, Atsugi 243-01, Japan
(Received 5 November 1991)

Charge-carrier transport in the presence of a nonequilibrium population of edge states is studied both theoretically and experimentally. The attention is focused on the temperature dependence of the inter-edge-state (IES) electron scattering and on nonlinear effects of the edge-state transport, both in the integer-quantum-Hall-effect regime. First, a theoretical analysis of the IES transition is developed, which explicitly considers the Fermi distribution function of electrons in edge states and takes account of both a long-range impurity scattering and the acoustical-phonon scattering. The analysis explains well the observed temperature dependence of the IES equilibration length in high-mobility $GaAs/Al_xGa_{1-x}As$ heterostructure devices when a smooth parabolic edge potential is assumed. Second, analysis of nonlinear transport across a potential barrier predicts an inverted population of electrons in edge states, which explains asymmetric energy dissipation around the barrier recently observed by other authors. Furthermore, the analysis predicts a nonlinear two-terminal resistance of the potential barrier, which provides a reasonable account for the experimentally observed resistance. Third, nonlinear effects are reported in which the edge states reorganize themselves in the presence of a nonequilibrium population of electrons. This leads to a population-dependent IES equilibration length, which accounts for an observed nonlinear Hall resistance which is asymmetric about $I=0$. The onset of the IES spontaneous acoustic-phonon emission is observed when the amplitude of the unequal population between relevant edge states exceeds a threshold. Finally, experimental evidence is presented to show that the maximum amplitude to which adjacent edge states can be unequally populated is limited to one-half the value of the Landau-level-energy spacing $\hbar\omega_c$.

I. INTRODUCTION

When a finite two-dimensional electron gas (2D EG) is subjected to high magnetic fields, the confining potential for the 2D EG causes Landau level energies to increase near the boundary of the 2D EG to form edge states.[1] Until recently, the edge states were not considered to play substantial roles in determining the electrical transport properties. This is chiefly because most theoretical studies of edge states assumed an infinitely sharp confining potential, which forces edge-state wave functions of different Landau levels to overlap significantly.[1-3] If the edge states are strongly mixed to establish a local equilibrium distribution of electrons at the boundaries,[3] the presence of edge states would not explicitly affect any aspects of the transport phenomena.

Recently, however, a number of transport phenomena have been reported in which edge states play crucial roles. A report by Hirai *et al.*[4] pointed out that the diagonal resistance in $GaAs/Al_xGa_{1-x}As$ heterostructure devices with a cross-gate structure largely deviates from the values predicted from a picture of local conductivity in the integer-quantum-Hall-effects (IQHE regime). The results apparently disagreed with the independent works of Haug *et al.*[5] and Washburn *et al.*,[6] who studied samples of a similar arrangement but obtained results not inconsistent with the picture of local conductivities.[4,7] A correct interpretation of the results of Ref. 4 has been provided by Komiyama *et al.*[7] and van Wees *et al.*[8] independently in experiments which demonstrated that the resistance is determined by the degree of coupling between electron reservoirs of the electrical contacts and edge states in a 2D EG. As has been pointed out theoretically by Büttiker,[9,10] electrons can be selectively injected into different edge states and selectively detected by disordered contacts. Disordered contacts can be either of a contact with a cross gate, a quantum point contact, or more generally, a contact with a finite contact resistance.[9-11] The nonlocal nature of resistance arises when the nonequilibrium population of edge states introduced by a disordered contact reaches another disordered contact serving as a voltage probe without equilibration. In particular, Refs. 7 and 11 have pointed out that a long distance in excess of 100 μm is necessary to equilibrate the population between the edge states of different Landau levels in the IQHE regime. The long-range nature of the nonequilibrium population between edge states has since become a subject of a number of recent experiments.[12-23] Possible deviations of the Hall resistance in the precision measurements of IQHE have been quantitatively analyzed in Ref. 16. Among all, Alphenaar *et al.* have studied in detail the dependence of the inter-edge-state (IES) equilibration length on different pairs of edge states, on magnetic field strength, and on filling factors.[23]

 ©1992 The American Physical Society

The long-range nature of the nonequilibrium population is further enhanced when the magnetic field departs from the regions of quantized Hall plateaus, as has been demonstrated by van Wees *et al.*[24] and subsequently studied by others.[25–31] Especially, McEuen *et al.* assumed the infinite equilibration length between the highest occupied Landau level and the other edge states, and proposed an ambitious model of the conductor which describes the conduction in magnetic fields outside the quantized Hall plateaus invoking solely the edge-state transport. The treatment of the highest occupied Landau level in this model has been criticized by van Son, de Vries, and Klapwijk[27] and Nii *et al.*,[30,31] and the McEuen model was modified to successfully explain anomalous Shubnikov–de Haas oscillations and Hall-step structures in high-mobility Hall-bar devices.[30,31]

When extremely long IES equilibration length was pointed out by Refs. 7 and 11, the concept of an extremely long IES equilibration length was hardly reconciled with the earlier belief of researchers which was strongly influenced by the conventional assumption of the sharp edge potential. To explain the extremely weak IES scattering, theories now propose to assume a slowly varying confining potential.[32] This latter assumption appears to have been widely accepted, at least, in the treatment of 2D EG in high-mobility devices.[33–35] It may be almost self-evident that the rate of IES scattering can be arbitrarily low if the relevant edge-state wave functions are sufficiently separated from one another in a very weak confining potential. In principle, however, there may be no *a priori* reason to rule out other possibilities of explaining the weak IES scattering. To make certain that this assumption is valid, it is therefore crucial to ask whether the smooth potential is consistent with other independent experimental observations. For instance, the present authors have reported that the experimentally observed temperature dependence of the IES equilibration length is consistent with a smooth potential.[19] The theoretical analysis of IES electron transition presented in Ref. 19 explicitly considered the Fermi distribution function of electrons in edge states. The analysis included a short-range impurity scattering and the acoustical-phonon scattering while taking the strength of an electron-phonon interaction as an adjustable parameter.[19] Alphenaar *et al.*, on the other hand, reported a different temperature dependence which does not fit existing theories based on a smooth potential.[23]

The first half of the present work treats this problem. In Sec. II, we improve the analysis presented in Ref. 19 by including a Gaussian-type long-range impurity scattering and by starting from the known deformation potential for the acoustical-phonon scattering. We describe the experimental arrangement in Sec. III. We report, in Sec. IV, the temperature dependence of the IES equilibration length in a regime of IQHE studied by using high-mobility $GaAs/Al_xGa_{1-x}As$ heterostructure devices with a cross gate. From a comparison between the theory and experiment in Sec. IV, we find that a slowly varying confining potential does explain the observed T dependence. Our analysis definitely shows that thermal broadening of the electron distribution function is of decisive importance in accounting for the T dependence, which has not been explicitly considered in existing theories.

Nonlinear transport effects are an important aspect inherent in the edge-state transport,[4,7,19–21] for which little has been clarified. To achieve a deeper understanding of the edge-state transport in general, the last half of this paper is devoted to a comprehensive description of nonlinear effects. In the theoretical part, the Landauer-Büttiker approach will be, in several aspects, extended to treat nonlinear transport. We will find that nonlinear effects manifest themselves through a variety of different mechanisms. In Sec. V A, we analyze nonlinear transport across a potential barrier and predict an inverted population of electrons to occur in an edge state when the electrochemical potential across a barrier differs by more than the Landau-level-energy spacing $\hbar\omega_c$. The analysis provides a reasonable account of an experimentally observed two-terminal resistance. Quantitative treatments of energy transport described in Sec. V B show that the predicted population inversion explains asymmetric energy dissipation around the barrier, recently observed by Klass *et al.*[36] In Sec. V C, we will show that edge states reorganize themselves when they are unequally populated, and this leads to a nonlinear four-terminal resistance which is asymmetric about $I=0$. Another important feature is the onset of spontaneous emission of acoustical phonons, which is observed when the difference in electrochemical potential between two edge states reaches the phonon energy needed to cause the IES transition. Finally, in Sec. V D, experimental evidence is presented to show that the amplitude of nonequilibrium population between adjacent edge states cannot exceed one-half the value of $\hbar\omega_c$.

II. ANALYSIS OF INTER-EDGE-STATE RELAXATION

A. General consideration

Throughout this work we deal with a regime of IQHE, where backscattering of electrons from one boundary of a sample to another boundary is neglected. Below we will relate IES electron scattering to the relaxation length over which the population of different edge states is equilibrated. Consider two edge channels of $i=0$ and 1 for which electrochemical chemical potentials at a location of y are slightly different; viz., $\mu_0=\varepsilon_F+\Delta\mu/2$ and $\mu_1=\varepsilon_F-\Delta\mu/2$, as shown in Fig. 1(a), where ε_F is the Fermi level. A net electron transfer occurs from the $i=0$ edge channel to the $i=1$ edge channel due to IES scattering. Let the net electron flux per unit length be $\partial n/\partial t$. Since the total current carried by the two edge channels must be conserved despite the IES electron transfer, the difference of electrochemical potential, $\Delta\mu$, decreases with the y coordinate (along the edge channel) as

$$d(\Delta\mu)/dy=-h\,\partial n/\partial t\ ,$$

where we have noted that the current carried by the ith edge channel changes by $(2e/h)d\mu_i$ when μ_i varies by $d\mu_i$, if the spin states are degenerated.[9,10,37,38] When the

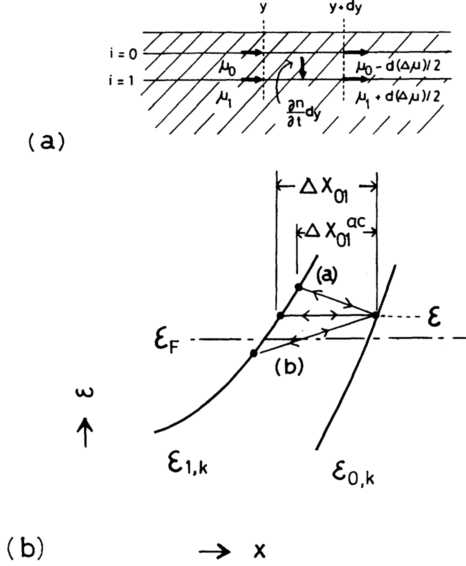

FIG. 1. (a) Change of the electrochemical potentials μ_0 and μ_1 of two edge states due to IES electron transfer $\partial n/\partial t$. (b) Spatial dispersion of $i=0$ and 1 edge states, and the IES separations, $\Delta X_{01}(\varepsilon)$ and $\Delta X_{01}^{\text{ac}}(\varepsilon)$, for elastic impurity scattering and for inelastic acoustical-phonon scattering. Two different processes, (a) and (b), are possible for the inelastic scattering, but only (a) is important.

amplitude of nonequilibrium population $\Delta\mu=\mu_0-\mu_1$, is sufficiently small, the electron flux $\partial n/\partial t$ is generally proportional to $\Delta\mu$. Hence, the equation above shows that $\Delta\mu$ decreases *exponentially*,

$$\Delta\mu(y)=\Delta\mu(0)\exp(-y/l) ,$$

with increasing the y coordinate, where the equilibration length,

$$l=[\Delta\mu/(\partial n/\partial t)]/h , \tag{1}$$

is a constant independent of $\Delta\mu$. The IES relaxation times for the $i=0$ and 1 edge channels are defined by the relations

$$l=\tau_{10}v_0=\tau_{01}v_1 ,$$

where v_i are the group velocities of the ith edge states at the Fermi level. We will consider acoustical-phonon scattering and impurity scattering for the IES transition. We apply Mathiessen's rule assuming that each scattering event is mutually independent:

$$l^{-1}=l_{\text{ac}}^{-1}+l_{\text{imp}}^{-1} ,$$

where l_{ac} and l_{imp} refer to the lengths determined by acoustical-phonon and impurity scattering processes, respectively.

Let us consider the one-electron Hamiltonian

$$H=p_x^2/2m^*+m^*\omega_c^2(x-X_n)^2/2+U(x) \tag{2}$$

to describe a 2D EG on the xy plane, which is confined by the electrostatic potential $U(x)$ under a magnetic field **B** applied along the z direction. Here, the Landau gauge $\mathbf{A}=(0,Bx,0)$ is used and $\omega_c=eB/m^*c$ is the cyclotron angular frequency with $m^*=0.067m_0$ (m_0 is the free-electron mass). The eigenstates

$$|i,k\rangle=\zeta(z)\phi_{i,k}(x-X_i)\exp(iky) \tag{3}$$

are specified by the Landau level index i and the wave number k along the y direction. The wave number k is related to the center coordinate of the wave function X_i through

$$X_i=-kl_B^2 , \tag{4}$$

where $l_B=(hc/eB)^{1/2}$ is the magnetic length. In this work, we will consider a slowly varying potential such that $dU/dx \ll \hbar\omega_c/l_B$. It follows that the center coordinate X_i given above well approximates the center of gravity of the wave function; viz., $X_i\simeq\langle i,k|x|i,k\rangle$. In the process of IES scattering between $|i,k_i\rangle$ and $|i+1,k_{i+1}\rangle$, the crystal momentum has to be conserved, so that the y component of the momentum

$$\hbar q_y=\hbar(k_{i+1}-k_i)=-\hbar\,\Delta X_{i,i+1}/l_B^2 \tag{5}$$

must be transferred from a scatterer, where $\Delta X_{i,i+1}=X_i-X_{i+1}$ is the spatial distance between the initial and final edge states.

It is an important feature of the IES scattering in a slowly varying edge potential that the necessary momentum transfer $\hbar q_y$ is relatively large because the distance $\Delta X_{i,i+1}$ is much larger than l_B. It follows that scattering by a long-range potential is significantly suppressed.[32,34,39] For a scatterer with a given force range, therefore, the transition probability is a decreasing function of $\Delta X_{i,i+1}$. This, in turn, implies that the probability of a long-range scattering increases with the energy, ε, of the relevant electron because $\Delta X_{i,i+1}$ is generally a decreasing function of ε. In addition, the overlapping integral between the edge-state wave functions exponentially decreases with increasing $\Delta X_{i,i+1}$. The probability of the IES transition is, again, strongly suppressed as $\Delta X_{i,i+1}$ increases due to this additional mechanism, as stressed by Martin and Feng.[32] Hence, at elevated temperatures, electrons thermally excited in a higher ε range of the edge states primarily contribute to the IES transition. To analyze the temperature dependence, it is thus essential to take explicitly into account the distribution function of electrons. Generally, the energy-dependent rate of the IES transition described above causes a nonequilibrium electron distribution *within* respective edge states. We assume, however, that the *intra-edge-state* scattering is efficient enough to establish the equilibrium Fermi distribution within the respective edge states; namely, we assume that

$$f_i(\varepsilon)=1/[1+\exp(\varepsilon-\mu_i)/kT]$$

for each edge channel.

To be specific, we will study three different types of confining potentials. The first one, which will be described in detail in this paper, is one of parabolic type, of the form

$$U(x)=\begin{cases}\frac{1}{2}m^*\omega_0^2x^2 & \text{for } x>0\\ 0 & \text{for } x<0\ .\end{cases} \quad (6)$$

In the limit of a smooth confinement, $\omega_0 \ll \omega_c$, the eigenenergies with a center coordinate of $X_i>0$ are nearly equal to those in the complete parabolic potential, which are given by[32,40,41]

$$\varepsilon_i(X_i)=(i+\tfrac{1}{2})\hbar\omega+(\omega_c/\omega)^2(m^*/2)\omega_0^2X_i^2\ , \quad (7)$$

with $\omega^2=\omega_c^2+\omega_0^2$. This is, in fact, a good approximation in our case, where $\omega_0/\omega_c=0.178$ or $\omega=1.016\omega_c$ will be derived from the analysis of our experimental results. The parameter ω_0 is related to the IES spacing at $\varepsilon=\varepsilon_F=2\hbar\omega$ through

$$\Delta X_{01}(\varepsilon_F)=(\sqrt{3}-1)(\omega/\omega_c)^{3/2}(\omega_c/\omega_0)l_B\ , \quad (8)$$

where

$$\Delta X_{01}(\varepsilon)=X_0(\varepsilon)-X_1(\varepsilon)\ . \quad (9)$$

We will use the notation $r(\varepsilon)=\Delta X_{01}(\varepsilon)/l_B$ and $r_0=\Delta X_{01}(\varepsilon_F)/l_B$ later. In the condition $\omega_0 \ll \omega_c$, the wave functions $\phi_{i,k}(x-X_i)$ in Eq. (3) are harmonic-oscillator functions centered at $x=(\omega_c/\omega)^2X_i\simeq X_i$, which are of the same character as those of the ideal bulk Landau levels.

The second type of confinement studied is a constant-slope potential, $U(x)=Cx$ $(x>0)$ and $U(x)=0$ $(x<0)$. This yields approximate eigenenergies of $\varepsilon_i(X_i)=(i+\frac{1}{2})\hbar\omega_c+CX_n$, for which IES separation is energy independent. With this type of dispersion, and according to an analysis similar to that described below, l_{imp} is temperature independent and l_{ac} is only weakly temperature dependent due to the T dependence of the occupation number of phonons. The experimentally observed large temperature dependence of l (Fig. 4) cannot be explained with any choice of C: namely, a calculation shows that an unrealistically large deformation potential (by more than one order of magnitude larger than the known value for GaAs) has to be assumed to explain the data. This definitely indicates that the actual dispersion of edge states is of such a character that the spacing ΔX_{01} decreases with ε, as in the case of Eq. (7). Thirdly, to examine a case where ΔX_{01} decreases with ε more rapidly than in the case of parabolic confinement, we have studied a hyperbolic-type potential described by $U(x)=-C/x$ $(x<0)$ with approximate eigenenergies of $\varepsilon_i(X_i)=(i+\frac{1}{2})\hbar\omega_c-C/X_i$. Calculations based on an analysis similar to that described below showed significant temperature dependence of l, but the overall fit of the theoretical curve of l vs T to the experimental one was not as excellent as that obtained from the parabolic-type dispersion. So, the energy dispersion as given by Eq. (7) is the most realistic one among the three types studied, and we will describe only the case of the parabolic-type dispersion below.

B. Acoustical-phonon scattering

The 2D EG in GaAs/$Al_xGa_{1-x}As$ heterostructures interacts with acoustical phonons through a short-range deformation potential as well as a long-range piezoelectric potential. The parameters determining strengths of these interactions have been obtained for GaAs from the temperature dependence of the electron mobility[42–44] as well as from independent experiments unrelated to charge transport. In our analysis, we neglect the piezoelectric interaction because of its long-range nature, and will only consider the deformation potential scattering, to which bulk longitudinal phonons in GaAs are relevant.[44]

Existing theories of the IES acoustical-phonon scattering do not provide convenient expressions for studying the ε dependence of the scattering rate in given edge states.[32,34] The probability of an inter-Landau-level transition due to an unscreened deformation potential scattering has been studied by Toombs *et al.* for ideal bulk Landau states.[45] Since the edge-state wave functions are of the identical character to those of the bulk Landau levels, we can start from the results of Ref. 45. As shown in the Appendix, the squared matrix elements for the IES transition $|0,k_0\rangle \rightarrow |1,k_1\rangle$ due to emission or absorption of a phonon of wave vector $\mathbf{q}=(q_x,q_y,q_z)$ are approximated as

$$|M_{10}^{\mathbf{q}}|^2=|\langle 1,k|H_{\text{ac}}|0,k_0\rangle|^2$$
$$=(\hbar E_d^2/4\rho Vc_sl_B)s_{\text{ac}}(n_{\text{ac}}+\tfrac{1}{2}\pm\tfrac{1}{2})\delta_{k_0-k_1,\pm q_y}$$

for $|q_x|\le(\pi/2)^{1/2}(1/l_B)$ and $|q_z|\le(3\pi/16)(1/a)$ with $a=35$ Å, and

$$|M_{10}^{\mathbf{q}}|^2=0 \quad \text{otherwise}\ , \quad (10)$$

where $\pm$ signs refer to emission and absorption processes, respectively, $E_d=9.3$ eV is the deformation potential of electrons in GaAs,[44] $\rho=5.3$ g/cm^3 is the density of GaAs,[43] $c_s=5.2\times10^5$ cm/s is the longitudinal sound velocity in GaAs,[41] and $V=L_xL_yL_z$ is the crystal volume. Here,

$$s_{\text{ac}}(\varepsilon)=r_{\text{ac}}^3\exp[-(r_{\text{ac}}^2/2)] \quad (11)$$

with $r_{\text{ac}}(\varepsilon)=\Delta X_{0,1}^{\text{ac}}/l_B$ a factor of the overlapping integral of the edge-state wave functions, which agrees with the Martin-Feng expression[32] and represents the suppression of the scattering probability. We explicitly treat the energy-dependent IES separation represented by

$$\Delta X_{01}^{\text{ac}}(\varepsilon)=X_0(\varepsilon)-X_1(\varepsilon\mp\varepsilon_{\text{ac}}) \quad (12)$$

as shown in Fig. 1(b). Here, the phonon energy $\varepsilon_{\text{ac}}=\hbar c_sq$ is approximated by $\hbar c_sq_y=\hbar c_s\,\Delta X_{01}^{\text{ac}}(\varepsilon)/l_B^2$ since $q_y \gg q_x,q_z$ as noted in the Appendix. The quantities ε_{ac} and $\Delta X_{01}^{\text{ac}}$ are determined by the simultaneous equations

$$\varepsilon_0(X_0)=\varepsilon,\quad \varepsilon_1(X_1)=\varepsilon\mp\varepsilon_{\text{ac}}\ ,$$
$$\text{and} \quad (13)$$
$$\varepsilon_{\text{ac}}(\varepsilon)=\hbar c_s\,\Delta X_{01}^{\text{ac}}/l_B^2\ ,$$

where $\varepsilon_n(X_n)$ are given by Eq. (7). In Eq. (10), n_{ac} is the phonon occupation number

$$n_{\text{ac}}=[\exp(\varepsilon_{\text{ac}}/kT)-1]^{-1}\ ,$$

which is an increasing function of the electron energy ε through $\varepsilon_{ac}(\varepsilon)=\hbar c_s \Delta X_{01}^{ac}/l_B^2$.

Let us consider those scattering processes in which the $0\rightarrow1$ transitions arise from phonon absorption and the $1\rightarrow0$ transitions arise from phonon emission, as shown by the arrow (a) in Fig. 1(b). Here,

$$\Delta X_{01}^{ac}(\varepsilon)=X_0(\varepsilon)-X_1(\varepsilon+\varepsilon_{ac})$$

and $\varepsilon_1=\varepsilon+\varepsilon_{ac}$. The electron flux from the $i=0$ edge channel to the $i=1$ edge channel due to phonon absorption is given by

$$\partial n_{10}/\partial t=\sum_{\mathbf{q}}\int_{\hbar\omega/2}^{\infty}d\varepsilon(2\pi/\hbar)|M_{01}^{\mathbf{q}}|^2 \times f_0(\varepsilon)[1-f_1(\varepsilon+\varepsilon_{ac})] \times D_0(\varepsilon)D_1(\varepsilon+\varepsilon_{ac})L_y ,$$

where $D_i(\varepsilon)=(1/\pi)|\partial\varepsilon_i/\partial k|^{-1}=(1/l_B^2\pi)|\partial\varepsilon_i/\partial X_i|^{-1}$ are the densities of states when spin states are degenerated. Using Eq. (10) and noting that the number of available phonon modes with $|q_x|\leq(\pi/2)^{1/2}(1/l_B)$ and $|q_z|\leq(3\pi/16)(1/a)$ is

$$4[L_xL_z/(2\pi)^2](\pi/2)^{1/2}(1/l_B)(3\pi/16)(1/a) ,$$

we rewrite $\partial n_{10}/\partial t$ to

$$\partial n_{10}/\partial t=(3\sqrt{2\pi}E_d^2)/(64\rho c_s a l_B^2) \times\int_{\hbar\omega/2}^{\infty}f_0(\varepsilon)[1-f_1(\varepsilon+\varepsilon_{ac})] \times D_0(\varepsilon)D_1(\varepsilon+\varepsilon_{ac})s_{ac}(\varepsilon)n_{ac}(\varepsilon)d\varepsilon . \quad (14)$$

The electron flux due to the $1\rightarrow0$ transitions via phonon emission is, after a similar procedure, given by

$$\partial n_{01}/\partial t=(3\sqrt{2\pi}E_d^2)/(64\rho c_s a l_B^2) \times\int_{\hbar\omega/2}^{\infty}f_1(\varepsilon+\varepsilon_{ac})[1-f_0(\varepsilon)]D_1(\varepsilon+\varepsilon_{ac}) \times D_0(\varepsilon)s_{ac}(\varepsilon)[n_{ac}(\varepsilon)+1]d\varepsilon . \quad (15)$$

Another type of process is shown by the arrow (b) in Fig. 1(b), in which $\varepsilon_1=\varepsilon-\varepsilon_{ac}$, and the $0\rightarrow1$ and $1\rightarrow0$ transitions arise from phonon emission and phonon absorption, respectively. The relevant spatial separations $\Delta X_{01}^{ac}=X_0(\varepsilon)-X_1(\varepsilon-\varepsilon_{ac})$ in these processes, however, are substantially larger than those in the former processes (a). Consequently, the transition is suppressed much more significantly and the contribution from these scattering processes is actually negligible.

The net electron flux, $\partial n/\partial t=\partial n_{10}/\partial t-\partial n_{01}/\partial t$, is given by Eqs. (14) and (15). When we consider the case of small $\Delta\mu$, where

$$|\Delta\mu| \ll kT ,$$

$f_i(\varepsilon)$ are approximated by

$$f_i(\varepsilon)=f(\varepsilon)\mp f(\varepsilon)[1-f(\varepsilon)](\Delta\mu/2kT) ,$$

where

$$f(\varepsilon)=1/[1+\exp(\varepsilon-\varepsilon_F)/kT]$$

and the $-$ and $+$ signs refer to the $i=0$ and 1 edge states, respectively. Noting also the relation

$$n_{ac}(\varepsilon)=[1-f(\varepsilon)]f(\varepsilon+\varepsilon_{ac})/[f(\varepsilon)-f(\varepsilon+\varepsilon_{ac})] ,$$

we find

$$\frac{\partial n}{\partial t}=(3\sqrt{2\pi}E_d^2)/(64\rho c_s a l_B^2)(\Delta\mu/kT) \times\int f(\varepsilon)[1-f(\varepsilon+\varepsilon_{ac})]D_0(\varepsilon)D_1(\varepsilon+\varepsilon_{ac}) \times s_{ac}(\varepsilon)n_{ac}(\varepsilon)d\varepsilon .$$

Equation (1) then gives the inverse equilibration length

$$l_{ac}^{-1}(T)=l_{ac0}^{-1}(kT)^{-1}\int F_{ac}(\varepsilon)C_{ac}(\varepsilon)S_{ac}(\varepsilon)n_{ac}(\varepsilon)d\varepsilon , \quad (16)$$

where

$$F_{ac}(\varepsilon)=f(\varepsilon)[1-f(\varepsilon+\varepsilon_{ac})] ,$$

$$C_{ac}(\varepsilon)=[D_0(\varepsilon)D_1(\varepsilon+\varepsilon_{ac})]/[D_0(\varepsilon_F)D_1(\varepsilon_F)] ,$$

$$S_{ac}(\varepsilon)=s_{ac}(\varepsilon)/s_{ac}(\varepsilon_F) ,$$

and

$$l_{ac0}^{-1}=[(3\sqrt{2\pi}hE_d^2)/(64\rho c_s a l_B^2)] \times s_{ac}(\varepsilon_F)D_0(\varepsilon_F)D_1(\varepsilon_F) .$$

The IES equilibration length $l_{ac}(T)$ can thus be evaluated by using only one parameter ω_0.

C. Impurity scattering

The mobility of a 2D EG in high-mobility modulation-doped $GaAs/Al_xGa_{1-x}As$ heterostructures is known to be determined by remote impurity scattering due to positively charged donors in the $Al_xGa_{1-x}As$ layer separated from the 2D EG by a spacer layer, and by background impurity scattering due to residual impurities in the spacer layer and in the pure GaAs layer.[42,43] The scattering potentials are supposed to be of a long-force range in both cases. In general, additional random potentials may be introduced at the boundaries of a 2D EG during fabrication procedure. The additional scattering potentials may also have a long-force range when the 2D EG channel is patterned by wet etching because the 2D EG is strongly depleted from the etched side face.

For the IES elastic scattering, those scattering potentials with relatively small force ranges may be selectively important. However we are unable to identify which origin among the above candidates is most effective. Hence, we simply assume a Gaussian form for the random potential,

$$V_i(\mathbf{r})\propto\exp-[(\mathbf{r}-\mathbf{r}_i)/A]^2 , \quad (17)$$

by taking the force range A as an adjustable parameter. Martin and Feng consider only the short-range potential ($A=0$).[32] The long-range potential is considered by Ot-

suki and Ono[39] and Badalian, Levinson, and Maslov,[34] but the derived expressions are not convenient for explicitly including the electron Fermi distribution function into the calculation. In our model we note that the probability for the long-range impurity scattering is suppressed due to the necessary momentum transfer given by Eq. (5). The factor of the suppression is given by[39]

$$s_A(\varepsilon)=\exp[-(rr_A)^2/4] , \tag{18}$$

where $r(\varepsilon)=\Delta X_{01}(\varepsilon)/l_B$ is the IES separation given by Eq. (9) and $r_A=A/l_B$ is the normalized force range. In addition, the probability is suppressed by the factor[32]

$$s(\varepsilon)=r^2\exp[-(r^2/2)] \tag{19}$$

due to the overlapping integral of the edge-state wave functions. We thus expect that the inverse equilibration length due to the elastic impurity scattering can be written in the form

$$l_{\text{imp}}^{-1}(T)=l_{\text{imp}}^{-1}(0)(kT)^{-1}\int_{\hbar\omega/2}^{\infty}F(\varepsilon)C(\varepsilon)S(\varepsilon)S_A(\varepsilon)d\varepsilon , \tag{20}$$

according to a consideration similar to the case of phonon scattering, where $l_{\text{imp}}(0)$ is the equilibration length at zero temperature,

$$F(\varepsilon)=f(\varepsilon)[1-f(\varepsilon)] ,$$

$$C(\varepsilon)=[D_0(\varepsilon)D_1(\varepsilon)]/[D_0(\varepsilon_F)D_1(\varepsilon_F)] ,$$

$$S(\varepsilon)=s(\varepsilon)/s(\varepsilon_F) ,$$

and

$$S_A(\varepsilon)=s_A(\varepsilon)/s_A(\varepsilon_F) .$$

For evaluating Eq. (20), we take $l_{\text{imp}}(0)$, A, and ω_0 as parameters.

III. EXPERIMENTAL CONFIGURATION

The experiments are made on modulation-doped $Al_{0.3}Ga_{0.7}As/GaAs$ heterostructure Hall-bar devices with a 1-μm-long aluminum front cross gate as shown in Fig. 2(a), which are similar to those used in previous work.[7,19] The 2D EG density is $n_s=3.4\times10^{11}$ cm^2 with a 4.2-K mobility of about 1.3×10^6 cm^2/V s. The heterostructure consists of a 1-μm-thick undoped GaAs layer, a 200-Å-thick undoped $Al_{0.3}Ga_{0.7}As$ spacer layer, a 900-Å-thick Si-doped $Al_{0.3}Ga_{0.7}As$ layer, and a top cap layer of 100-Å-thick Si-doped GaAs. The 2D EG is photolithographically patterned by a deep chemical etching of the mesa structure (2000 Å deep from the top surface of the GaAs cap layer), into a 30-μm-wide standard Hall bridge. The distance between the gated 2D EG region and the adjacent side voltage probes along the 2D EG boundary is 55 μm. The electrical contacts are prepared with a conventional alloying technique but display relatively large contact resistances ($0.6\sim8$ kΩ at $B=3.7$ T),[10-12] probably because the alloying temperature was not optimum. These disordered contacts enable us to study

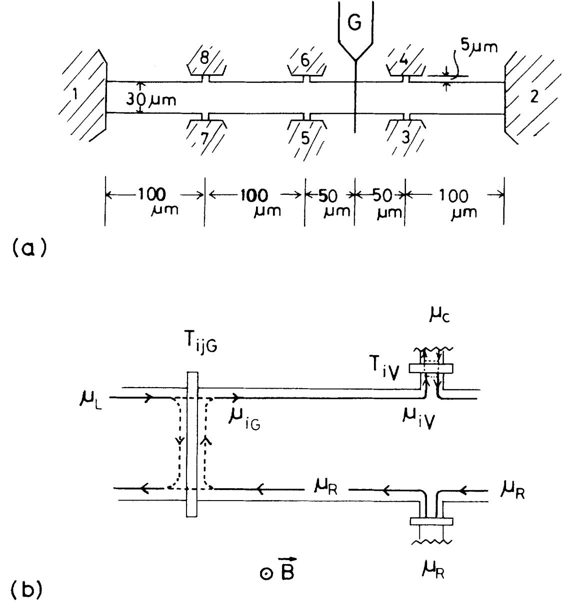

FIG. 2. (a) Schematic of the Hall-bar sample with a 1-μm-long cross gate. (b) Transmission and reflection of electrons at the potential barrier underneath the gate and at a disordered voltage probe.

nonequilibrium population of edge states quantitatively. Throughout the present studies, the current is passed between contacts 1 and 2 in magnetic fields pointing out of the page of Fig. 2, unless otherwise mentioned.

The complete analysis of a four-terminal resistance with arbitrary pairs of voltage probes from contact 3 to contact 8 in the present configuration is described in Ref. 12 by using the Landauer-Büttiker approach.[9,10] Here we briefly describe the essence of the present measurements to interpret the temperature dependence shown in Sec. IV. We consider a two-channel case where opposite spin states are degenerated in each channel. The electron current I is passed through the sample from the left-hand side to the right-hand side in Fig. 2(b). Suppose that the edge channels incident on the gated region from the left- and from the right-hand sides are, respectively, in equilibrium states characterized by the electrochemical potentials μ_L and μ_R. Here, we will be concerned with the linear transport regime, where $\mu_L-\mu_R$ is sufficiently small so that dependence on the electron energy of the transmission probabilities introduced below is negligible. Letting T_{ijG} be the probabilities for electrons incident on the potential barrier beneath the gate along the jth edge channel from the left to be transmitted in the ith edge channel to the right, the total current passed through the barrier is given by

$$I=(2e/h)T_G(\mu_L-\mu_R) , \tag{21}$$

where $T_G=T_{0G}+T_{1G}$ is the total transmission probability with $T_{iG}=T_{i0G}+T_{i1G}$. The edge channels at the upper right corner of the gated 2D EG region are unequally occupied to have the chemical potentials of $\mu_{iG}=T_{iG}\mu_L+(1-T_{iG})\mu_R$ or

$$\mu_{iG}=(1\pm\gamma)(h/4e)I+\mu_R \ , \tag{22}$$

where $\pm$ signs are for the $i=0$ and 1 edge channels, and

$$\gamma=(T_{0G}-T_{1G})/T_G \tag{23}$$

characterizes the selective scattering of different edge channels by the potential barrier. Parameter γ varies in the range $0\leq\gamma\leq 1$ according to a gate bias condition. Note that the unequal population

$$\Delta\mu_G\equiv\mu_{0G}-\mu_{1G}=\gamma(h/2e)I \tag{24}$$

reverses its sign when the polarity of current I is reversed. Note also that a similar unequal population is introduced at the lower left corner of the gated 2D EG region. The sign of $\Delta\mu_G$ at this diagonally opposite corner is opposite for a given polarity of current.

The degree of unequal occupation of edge states decreases as the edge current travels along a sample boundary due to IES scattering. Suppose $\Delta\mu_G$ is reduced to $\Delta\mu_V=\beta\,\Delta\mu_G$ $(0\leq\beta\leq 1)$ at the entrance of the voltage probe. When $\Delta\mu_G$ is sufficiently small, β can be written as $\beta=\exp(-L/l)$, by using an equilibration length l as shown in the last section, where $L=55$ μm is the sample-boundary length between the gated region and the voltage probe. The electrochemical potentials of the ith edge channel at the voltage probe are

$$\mu_{iV}=(1\pm\gamma\beta)(h/4e)I+\mu_R \ . \tag{25}$$

The electrochemical potential μ_c of the electron reservoir in the voltage probe is given by $\mu_c=(T_{0V}\mu_{0V}+T_{1V}\mu_{1V})/T_V$ or

$$\mu_c=(1+\gamma\beta\alpha)(h/4e)I+\mu_R \ . \tag{26}$$

Here T_{iV} and $T_V=T_{0V}+T_{1V}$ are the probabilities relevant to the voltage probe contact, and

$$\alpha=(T_{0V}-T_{1V})/T_V \tag{27}$$

characterizes the selective detection of edge channels by the voltage probe. Parameter α can take a contact-specific value in the range $|\alpha|\leq 1$. The Hall voltage $V_H=(\mu_c-\mu_R)/e$ deviates from the quantized value $(h/4e^2)I$ by

$$\Delta V_H=\gamma\beta\alpha(h/4e^2)I \ . \tag{28}$$

The Hall resistance thus deviates from the quantized value by $\Delta R_H=\gamma\beta\alpha(h/4e^2)$.

IV. TEMPERATURE DEPENDENCE

A. Experimental results and comparison with theory

The solid lines in Fig. 3 display the dependence of the Hall resistance $R_{3,4}=V_{3,4}/I=(\mu_c-\mu_R)/(eI)$ on the gate bias voltage V_G at different temperatures T.[19] The voltage difference between contacts 3 and 4 is studied with a lock-in amplifier while an ac current (10 Hz) of a 2-nA amplitude is transmitted. The dashed line shows the four-terminal resistance $R_{3,6}$ at $T=1.65$ K, which is, physically, the two-terminal gate resistance

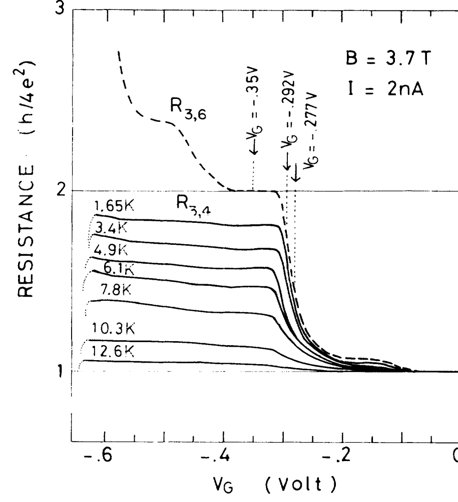

FIG. 3. The Hall resistance $R_{3,4}=V_{3,4}/I$ vs gate bias voltage at different temperatures, together with $R_{3,6}=V_{3,6}/I$ at $T=1.6$ K.

$$R_{3,6}=V_{3,6}/I=(\mu_L-\mu_R)/(eI)$$
$$=(1/T_G)(h/2e^2) \ .$$

The magnetic field strength ($B=3.7$ T) corresponds to the center of the Hall plateau of the Landau-level filling factor ν of 4 in the ungated region of the 2D EG. With decreasing the gate bias voltage V_G with respect to the 2D EG, a potential barrier is formed underneath the gate, and γ changes from 0 ($T_{0G}=T_{1G}=1$) to 1 ($T_{0G}=1, T_{1G}=0$). As a consequence, the Hall resistance deviates from the quantized value, $h/4e^2$, to yield a shifted plateau with decreasing V_G. The current $I=2nA$ is so small that $\Delta\mu_G=(h/2e)I=0.026$ meV is far smaller than kT even at the lowest temperature studied. Hence, noting Eq. (28) with $\beta=\exp(-L/l)$, we can express the deviation of the Hall resistance at the shifted plateau as $\Delta R_H=\alpha[\exp(-L/l)](h/4e^2)$. At the lowest temperature, the deviation at the plateau amounts to 0.83 $h/4e^2$. This is direct proof that the equilibration length l is larger than 295 μm at $T=1.65$ K because α cannot be larger than unity. (Also, $0.83\leq\alpha$ is derived.)

At a fixed gate bias voltage of $V_G=-0.35$ V, ΔR_H decreases with increasing temperature up to 12.6 K. This implies that either the equilibration length of edge states, l, or the selectivity of the voltage probe, α, decreases with increasing temperature. To distinguish theses two, we have carried out similar measurements using other voltage probes including other devices. Although the absolute amplitude of ΔR_H largely depended on particular voltage probes as reported in Ref. 15, the temperature dependence of ΔR_H was found to be independent of the probes. Also, we have confirmed that the contact resistance,[10] $R_c=[(2/T_V)-1]h/4e^2$, of the voltage probes does not change appreciably with T in the temperature range studied. These two facts indicate that α of each voltage probe is T independent. Hence, the inverse equilibration length can be deduced from the observed

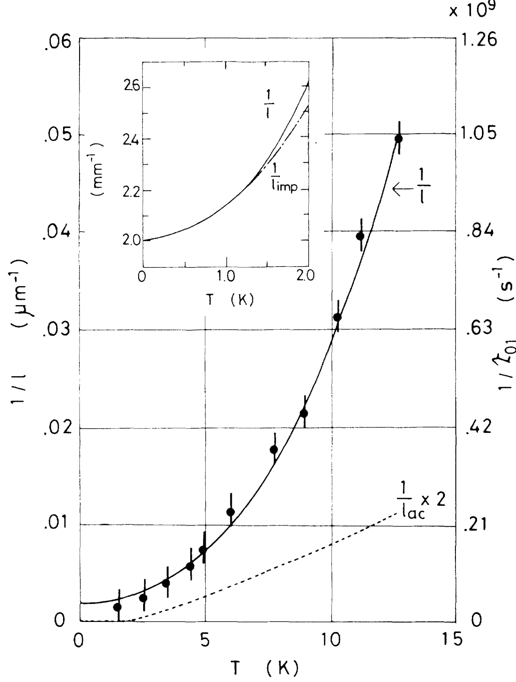

FIG. 4. The inverse equilibration length between the $i=0$ and 1 edge states. The solid line $1/l=1/l_{ac}+1/l_{imp}$ and the dotted line $1/l_{ac}$ indicate theoretical values [Eqs. (16) and (20)] with $\omega_0=1.69\times10^{12}$/s, $A=157$ Å ($r_A=1.21$), and $l_{imp}(0)=500$ μm. The dash-dotted line in the inset shows theoretical values of $1/l_{imp}$.

$\Delta R_H(T)$ at $V_G=-0.35$ V by using the relation

$$1/l=(1/L)\{-\ln[\Delta R_H/(h/4e^2)]+\ln\alpha\}\ , \qquad (29)$$

which is derived from the expression of ΔR_H. Actually, parameter γ of the gate slightly decreases from $\gamma=1$ with increasing T, supposedly because T_{1G} becomes finite at elevated temperatures. Although not described here, we have determined $\gamma(T)$ from a T dependence of the two-terminal resistance R_{36} and corrected the data to derive $1/l$. The result is plotted as a function of T with solid dots in Fig. 4. Error bars of the data points reflect the arbitrariness in α; viz., $0.83\le\alpha\le1$. The equilibration length, which is larger than about 300 μm at the lowest temperature, is reduced to about 20 μm at 12.6 K.

The data of $1/l$ can be compared to theoretical values $1/l=1/l_{imp}+1/l_{ac}$ calculated with Eqs. (16) and (20). As shown by a solid line in Fig. 4, the calculation well reproduces the experimental data when parameter values $l_{imp}(0)=500$ μm, $A=157$ Å, and $\omega_0=1.69\times10^{12}$/s are used. The dotted line indicates the fractional contribution from the acoustical-phonon scattering and shows that the major contribution arises from impurity scattering. Under the restriction of $l_{imp}(0)>300$ μm, arbitrariness in the choice of parameter values is practically not large. The small ratio of ω_0 to ω_c ($\omega_0/\omega_c=0.174$) validates the approximations we have made in the theoretical analysis of Sec. II. The energy separation $\hbar\omega=\hbar\sqrt{\omega_c^2+\omega_0^2}=1.016\hbar\omega_c$ between the two Landau levels at the edge, given in Eq. (7), is very close to $\hbar\omega_c$. The IES separation is derived to be $r_0=4.2$ through Eq. (8). The group velocities of electrons in the $i=0$ and 1 edge channels, $v_i=\hbar^{-1}|\partial\varepsilon_{i,k}/\partial k|_{\varepsilon_F}$, are $v_0=3.7\times10^6$ cm/s and $v_1=2.1\times10^6$ cm/s. The inverse of the IES relaxation time, $1/\tau_{01}=v_1/l$, is indicated by the scale on the right-hand side of Fig. 4. Important parameters characterizing the edge states are summarized in Table I.

The observed long IES equilibration length at low temperatures is completely consistent with the here determined large separation r_0 between edge states. For example, the suppression factors of the scattering are $s_{ac}(\varepsilon_F)=1.0\times10^{-2}$, $s(\varepsilon_F)=2.6\times10^{-3}$, and $s_A(\varepsilon_F)=1.6\times10^{-3}$. Considering the low-magnetic-field mean free path l_m of electrons (estimated to be 10 μm) together with these suppression factors, the observed size of l is not surprisingly large. It is difficult, however, to relate l to l_m because (a) the screening effect of impurity potentials may largely differ in the presence of a quantizing magnetic field and (b) additional unknown random potentials may be present at the boundaries of the 2D EG.

Figures 5 and 6 elucidate the origin of the T dependence in l_{imp} and l_{ac}. Figure 5 displays characteristic quantities relevant to impurity scattering as a function of electron energy ε. The transition probability due to impurities increases rapidly with increasing electron energy ε because both $S(\varepsilon)$ and $S_A(\varepsilon)$ drastically increase with ε due to the decrease of IES separation $r(\varepsilon)$ as shown in Fig. 5(a). On the other hand, the reduction with ε in the combined density of states, $C(\varepsilon)$, is relatively slow. Hence, the broadening of the Fermi distribution function $F(\varepsilon)$ with increasing T as shown in Fig. 5(b) causes a

TABLE I. Characteristic parameters of the edge states and of the IES scattering, determined by the analysis. Here, ω_0, $l_{imp}(0)$, and $r_A=A/l_B$ are given, respectively, by Eqs. (6), (20), and (17). The normalized IES separation $r_0=\Delta X_{01}(\varepsilon_F)/l_B$, the group velocities of edge states $v_i=\hbar^{-1}|\partial\varepsilon_{i,k}/\partial k|_{\varepsilon_F}$, and the phonon energy $\varepsilon_{ac}(\varepsilon_F)$ relevant to an IES transition given by Eq. (13) are derived from ω_0. Parameters used for the analysis are the effective mass of electrons $m^*=0.067m_0$, the deformation potential $E_d=9.3$ eV (Ref. 44), the density $\rho=5.3$ g/cm^3 of GaAs (Ref. 43), and the longitudinal sound velocity $c_s=5.2\times10^5$ cm/s of GaAs (Ref. 43). The magnetic length is $l_B=\sqrt{\hbar c/eB}=130$ Å and the cyclotron angular frequency is $\omega_c=9.7\times10^{12}$/s in the magnetic field of $B=3.7$ T.

ω_0 (s^{-1})	$l_{lim}(0)$(μm)	r_A	r_0	v_0 (cm/s)	v_1 (cm/s)	$\varepsilon_{ac}(\varepsilon_F)$ (meV)
1.69×10^{12}	500	1.21	4.2	3.7×10^6	2.1×10^6	0.95

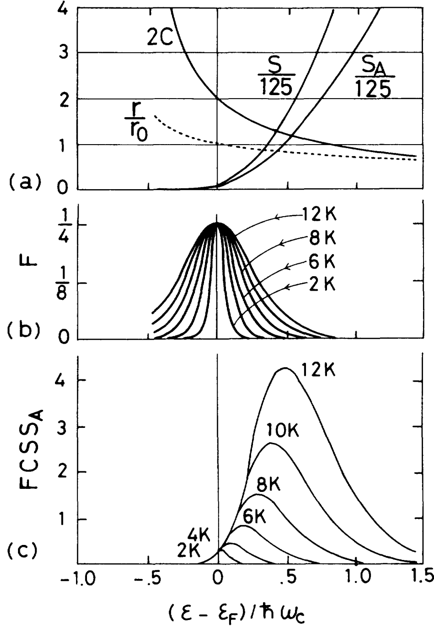

FIG. 5. Dependence on electron energy of characteristic quantities in the elastic impurity scattering.

significant increase with T of the integrand $FCSS_A$ in Eq. (20) as shown in Fig. 5(c). Note that the T dependence of $l_{\rm imp}$ does not vanish at $T=0$. When T is sufficiently low, the only relevant thing is a small energy interval around $\varepsilon=\varepsilon_F$ in which SS_A can be approximated by a linear term in ε; viz.,

FIG. 6. Energy dependence of characteristic quantities in the inelastic acoustical-phonon scattering, where ε is the electron energy in the $i=0$ edge channel.

$$SS_F=1+[\partial(SS_A)/\partial\varepsilon]_{\varepsilon_F}(\varepsilon-\varepsilon_F) .$$

This leads to a linear T dependence of $1/l_{\rm imp}$ in the limit of low T as shown in the inset of Fig. 4. Figure 6 elucidates similar data for the acoustical-phonon scattering. The overlapping integral $S_{\rm ac}(\varepsilon)$ increases rapidly with ε due to the decrease in $r_{\rm ac}(\varepsilon)$ as shown in Fig. 6(a). In addition, the phonon occupation number, $n_{\rm ac}(\varepsilon)$, increases with ε as shown in Fig. 6(b). The occupation number $n_{\rm ac}$ increases with increasing T. These, together with the broadening of the Fermi distribution function [Fig. 6(c)] with increasing T, lead to the growth of the integrand $F_{\rm as}C_{\rm ac}S_{\rm ac}n_{\rm ac}$ in Eq. (16), as shown in Fig. 6(d). In contrast to the impurity scattering, the contribution from phonon scattering vanishes in the limit of low T because $n_{\rm ac}$ vanishes.

We should note that the short-range impurity potential ($A=0$) is not capable of explaining the observed T dependence. On the assumption of $A=0$, the temperature dependence of $l_{\rm imp}$ is less significant because S_A is fixed to unity. Although a good fit between the experiment and the calculation was obtained with $A=0$ by assuming $l_{\rm ac0}=3680$ μm,[19] the assumed value of $l_{\rm ac0}$ corresponds to an electron–acoustical-phonon interaction ($E_d=45$ eV) much stronger than the known interaction ($E_d=9.3$ eV). The force range of $A\sim160$ Å derived in the present analysis may be reasonable if remote impurities separated from the 2D EG by the spacer layer thickness (200 Å) dominate the elastic scattering.[34]

B. Discussion

Berggren, Roos, and van Houten[46] derived $\omega_0'=2.3\times10^{12}$/s by analyzing Shubunikov–de Haas oscillations in a narrow GaAs/Al$_x$Ga$_{1-x}$As mesa structure under the assumption of a parabolic confining potential $\frac{1}{2}m^*\omega_0'^2x^2$. The mesa structure is similar to ours with a spacer layer thickness of 180 Å. To compare with our result, we should note that the effective width of the 2D EG channel in the Berggren, Roos, and van Houten work ($W\sim1400$ Å) is far smaller than the width of our sample ($W=30$ μm). In such a narrow sample, the influence of a confining potential on one boundary of the sample will reach the other boundary to have an effect to strengthen the effective confinement. In the case when a confining potential at a boundary of a wide sample is described by a half-parabola with ω_0, the confining potential in a narrow sample will be enhanced to $\omega_0'=\sqrt{2}\omega_0$ because, most simply considered, the potential is the superposition of respective potentials originating at the opposite boundaries:

$$U(x)=\tfrac{1}{2}m^*\omega_0^2[(x-X_b)^2+(x+X_b)^2]$$

$$=\tfrac{1}{2}m^*(\sqrt{2}\omega_0)^2(x^2+X_b^2) ,$$

where the bottoms of the respective potentials $x=\pm X_b$ are located outside the 2D EG channel. Thus, our value $\omega_0=1.69\times10^{12}$/s for a wide sample very closely corre-

sponds to $\omega_0'=2.3\times10^{12}$/s in narrow samples.

Alphenaar *et al.* reported that the inverse equilibration length $1/l$ linearly increases with temperature T in the low-T range of $0.5<T<4.2$ K.[23] Our theoretical model does not predict the T linear dependence except in a still lower T range below 0.5 K. It is important to note that the experiments of Alphenaar *et al.* apply $I=50$ nA for the amplitude of current, which corresponds to $\Delta\mu_G=0.7$ meV that is much larger than $kT=0.04$ meV at $T=0.5$ K. The "effective equilibration length" observed in such a condition ($\Delta\mu\gg kT$) is not the equilibration length considered in Sec. II. When $\Delta\mu\ll kT$, the energy interval primarily relevant to the IES electron transition is about $\pm kT$ around ε_F as shown in Fig. 7(a) and the T-dependent energy interval causes the T dependence of l as discussed in Sec. II and in the above. If $\Delta\mu\gg kT$, however, the relevant energy interval is nearly fixed to $\pm\Delta\mu/2$ around ε_F, being substantially independent of T as schematically shown in Fig. 7(b). Since the phonon scattering is not significant in the low-T range, it follows that our model generally predicts that the effective l should be substantially independent of T when $\Delta\mu\gg kT$. This apparently contradicts the result of the experiments of Alphenaar *et al.*, and leads us to suggest the following. First, the evaluation of $s_A(\varepsilon)$ and $s(\varepsilon)$ given by Eqs. (18) and (19) with the parameter values given in Table I shows that the rate of IES impurity scattering at $\varepsilon=\varepsilon_F+\Delta\mu/2$ is by several orders of magnitude larger than the one at $\varepsilon=\varepsilon_F-\Delta\mu/2$ when $\Delta\mu=0.7$ meV. Thus, IES equilibration occurs by a factor of several orders faster in the higher-ε range. This ε-dependant IES transition does not affect our prediction above if, as we have postulated in Sec. II, the *intra-edge-state* scattering is so efficient as to establish local equilibrium in respective edge states. This assumption, however, may not be self-evident at low T. Recent experiments on Coulomb-blockade oscillations[47,48] strongly suggest that the phase-coherence length, l_ϕ, of electrons in edge channels is extremely long in a regime of IQHE at low T.[49] We speculate that inelastic electron-electron scattering is the major origin for both l_ϕ and the intra-edge-state equilibration length $l_{\rm intra}$ at low T, and expect that $1/l_{\rm intra}$ reduces to zero at $T=0$. Hence, it is possible that $l_{\rm intra}>l$ at low T. In the condition of $\Delta\mu\gg kT$ and $l_{\rm intra}>l$, a lower-energy range $\varepsilon\sim\varepsilon_F-\Delta\mu/2$ of edge states will be left unequilibrated for a longer distance, roughly given by $l_{\rm intra}$. Hence, we suggest that the "effective equilibration length" $l_{\rm eff}$ experimentally observed in such a condition is substantially determined by the *intra-edge-state* equilibration ($l_{\rm eff}\sim l_{\rm intra}$). We thus suggest to interpret the observation of Alphenaar *et al.* as a consequence of the relation $1/l_{\rm intra}\propto T$.

Let us examine another assumption of our model. Our model postulated that the edge potential $U(x)$ remains unaltered when T increases. This is an approximation not rigorously guaranteed. Electrons and holes are thermally excited above and below ε_F as T increases. These thermally excited electrons and holes polarize each edge state as shown in Fig. 8 and modify the edge potential $U(x)$ as well as the edge states $\varepsilon_{i,k}(x)$, as will be discussed in detail for a somewhat different situation in Sec. V C. Such a rearrangement of edge states is more significant for the $i=1$ edge state than for the $i=0$ edge state because the density of states is larger in the $i=1$ edge state. Hence, the IES separation, $\Delta X_{01}(\varepsilon)$, for $\varepsilon>\varepsilon_F$ slightly increases with increasing T as schematically shown on the top of Fig. 8. This effect is expected to weaken the T dependence of $1/l$. Quantitatively, however, our preliminary estimation can show that this effect does not significantly affect the presently derived results in the T range studied.

The spin-up and spin-down bands with a same Landau-level index are strongly mixed at the edge states in a 2D EG of $GaAs/As_xGa_{1-x}As$ heterostructures, as has been shown experimentally[14,23] and assumed in this work. The strong spin-flip IES scattering ($i\uparrow\leftrightarrow i\downarrow$) suggests an important role of the spin-orbit interaction.[31] van Son, Wang, and Klapuijk[22] have recently discovered strikingly different features in Si-MOSFET's (metal-oxide-semiconductor field-effect transistor), where the equilibration length between the edge states of different Landau indexes with a same spin polarization, $l_{i\uparrow,(i+1)\uparrow}$, is relatively small while that for the opposite spin states with a same Landau index, $l_{i\uparrow,i\downarrow}$, is much larger. This cannot be explained in terms of the IES separation because $\Delta X_{i\uparrow,(i+1)\uparrow}\gg X_{i\uparrow,i\downarrow}$. Probably, a short $l_{i\uparrow,(i+1)\uparrow}$ is a consequence of a strong short-range impurity scattering in Si-MOSFET's. The longer $l_{i\uparrow,i\downarrow}$, on the other hand,

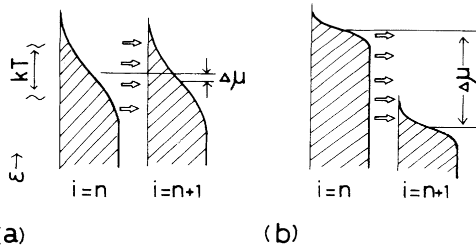

FIG. 7. Schematic representations of the electron distribution functions in the case of (a) $\Delta\mu\ll kT$ and in the case of (b) $\Delta\mu\gg kT$.

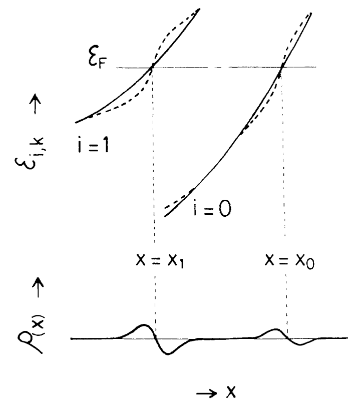

FIG. 8. Expected polarization of edge states and a resultant rearrangement of edge states at elevated temperatures.

suggests that, in spite of the significant overlapping of the edge-state wave functions, the spin-flip transition is nearly forbidden because of a very weak spin-orbit interaction for the inversion layer electrons in Si-MOSEFT's.[31] Therefore, the temperature dependence of the nonequilibrium population in this material should be described in a way other than the present approach.

V. NONLINEAR EFFECTS

Nonlinear properties of the related transport phenomena have been stressed already in Ref. 4. This remarkable nonlinearity turned out to be an inherent aspect of the edge-state transport.[7,19–22] A distinct characteristic of the nonlinearity here is its occurrence at a very low current level, say, $I < 1\ \mu$A. Another important feature is that the nonlinear behavior does not scale with the width W of the sample, but is described by the absolute magnitude of current. On the other hand, IQHE is known to be destroyed with large currents in standard Hall-bar devices.[50–52] A characteristic of this breakdown, observed at many groups on samples with different scales, is that the critical currents scale linearly with W. For instance, the critical current density for the $\nu=4$ Hall plateau ($B=3-4$ T) is about 6 mA/cm. This phenomenon can be explained in terms of an abrupt increase in the electron effective temperature.[52–54] This breakdown phenomenon is observed to occur also in the present devices at a current of about 20 μA (7 mA/cm), which is far larger than the current levels of the nonlinear effects discussed below. The phenomenon is almost independent of the gate bias condition. We should note, therefore, that the effects discussed are the phenomena physically unrelated to the well-known breakdown. Molenkamp *et al.* studied nonlinear effects in a narrower sample with $W=4\ \mu$m.[21] Special care must be taken in these experiments because nonlinear effects of the two different categories coexist at similar current levels.

Below we will deal with the case where $\Delta\mu \sim \hbar\omega_c \gg kT$. The experiments will be restricted to low temperatures, where IES phonon scattering can be neglected in the case of linear transport. Therefore, we will consider below only the absolute zero temperature for simplicity.

A. Energy-dependent transmission at a potential barrier

Preceding sections implicitly assumed that the transmission probabilities T_{iG} are independent of electron energy ε because the relevant energy interval is small. In the case of $\Delta\mu \sim \hbar\omega_c$, we have to explicitly consider the energy dependence of T_{iG}. Imagine that a potential barrier is jointed to ideal leads connecting to electron reservoirs on the left- and on the right-hand sides. Let the electrochemical potentials be μ_L and μ_R, respectively. (We assume $\mu_L > \mu_R$.) We consider the situation where N Landau levels ($i=0,1,\ldots,N-1$) are occupied in the ideal leads. Figure 9(a) schematically shows a landscape of a simplified potential barrier with equipotential contours. Since all the states with the energies below μ_R are completely filled, we only need to consider transmission or reflection of right-going electrons incident on the barrier with the energies $\mu_L \geq \varepsilon \geq \mu_R$. If the electrostatic potential $U(x,y)$ is slowly varying, a quasiclassical consideration is possible; an electron in the ith Landau level with energy ε is propagated along the equipotential contour determined by $\varepsilon=(i+\frac{1}{2})\hbar\omega_c+U(x,y)$. Let us represent by U_s the potential at the saddle point of the barrier. Since the equipotential contours with $U(x,y) > U_s$ extend to the other side of the barrier while those with $U(x,y) < U_s$ are reflected at the barrier, the probability for an electron of energy ε in the ith edge channel to be transmitted across the barrier has the simplified energy dependence given by

$$T_i(\varepsilon)=\begin{cases}1 & \text{for } \varepsilon > \varepsilon_i ,\\ 0 & \text{for } \varepsilon < \varepsilon_i ,\end{cases}$$

where

$$\varepsilon_i=(i+\tfrac{1}{2})\hbar\omega_c+U_s$$

is the threshold energy for the ith edge channel. Actually, $T_i(\varepsilon)$ smoothly varies from one to zero due to the tunneling transition at the saddle point, but the simplification above will suffice for the present discussion

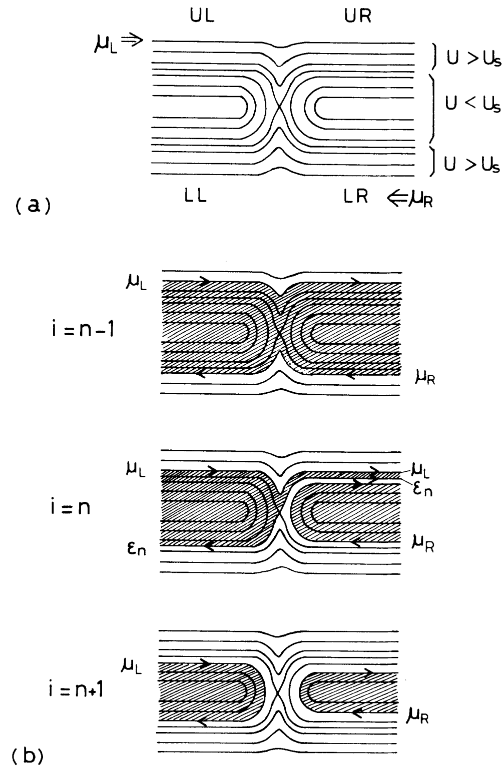

FIG. 9. (a) Equipotential contours of a simplified potential barrier. (b) Transmission and reflection of electrons in the $i=n-1$, $i=n$, and $i=n+1$ Landau levels in a nonlinear regime. The situation corresponds to case (i) in Fig. 10(b). The shadings indicate the regions occupied by electrons. A population inversion forms in the $i=n$ edge state at the UR boundary.

because the energy range over which perfect transmission changes to perfect reflection is far smaller than $\hbar\omega_c$.[55] The landscape of the potential barrier in actual experiments may be complicated. Nevertheless, $T_i(\varepsilon)$ for any potential barrier should have threshed energies ε_i differing by $\hbar\omega_c$ for adjacent Landau levels, so long as the potential barrier is smoothly varying. Therefore, we can always find the saddle-point potential U_s that gives the threshold energy through the relation $\varepsilon_i=(i+\frac{1}{2})\hbar\omega_c+U_s$.

For a given potential barrier, we can find such an integer n $(n\le N-1)$ for which $\varepsilon_F<\varepsilon_n<\varepsilon_F+\hbar\omega_c$, where $\varepsilon_F=(\mu_L+\mu_R)/2$ is the Fermi energy. If the difference in the electrochemical potential $\Delta\mu=\mu_L-\mu_R$ is smaller than $\hbar\omega_c$, it is possible to satisfy both of the relations

$$\mu_R>\varepsilon_{n-1} \tag{30}$$

and

$$\mu_L<\varepsilon_n\ , \tag{31}$$

as illustrated in Fig. 10(a). It follows that all the electrons having the energies $\mu_R\le\varepsilon\le\mu_L$ in the edge channels of $0\le i\le n-1$ are transmitted, while those in the edge channels of $n\le i$ are completely reflected. In this case, the system is in a regime of linear transport because the total transmitted current is given by $I=n(2e/h)\Delta\mu$ with the unchanged two-terminal resistance $R=\Delta\mu/eI=(1/n)(h/2e^2)$. The fashion of the electron population in the $i=n$ and $n-1$ edge channels at different boundaries are schematically shown in Fig. 10(a), where UL, LL, UR, and LR refer to the upper left, lower left, upper right, and lower right boundaries of the potential barrier shown in Fig. 9(a).

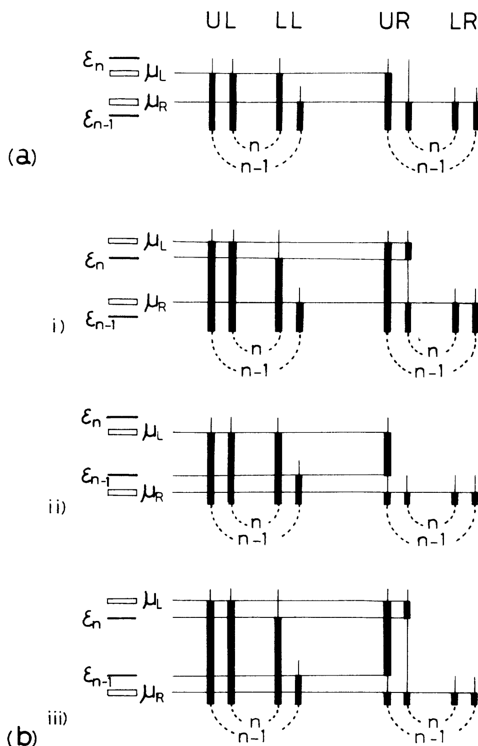

FIG. 10. Marked on the left-hand side are the threshold energies ε_n and ε_{n-1} for the transmission of electrons in the $i=n$ and $n-1$ Landau levels, together with μ_L and μ_R. The drawings indicate the electron population in the $i=n$ and $n-1$ edge states at different boundaries of the potential barrier specified in Fig. 9(a). (a) A linear regime; $\varepsilon_{n-1}<\mu_R<\mu_L<\varepsilon_n$. (b) Nonlinear regimes $\mu_L-\mu_R>\hbar\omega_c$, where $\varepsilon_{n-1}\le\mu_R<\varepsilon_n<\mu_L$ in case (i), $\mu_R<\varepsilon_{n-1}<\mu_L\le\varepsilon_n$ in case (ii), and $\mu_R<\varepsilon_{n-1}<\varepsilon_n<\mu_L$ in case (iii).

It is impossible to simultaneously satisfy both of the inequality relations (30) and (31) if $\Delta\mu>\hbar\omega_c$. We have three possible cases: (i) $\varepsilon_{n-1}\le\mu_R<\varepsilon_n<\mu_L$, (ii) $\mu_R<\varepsilon_{n-1}<\mu_L\le\varepsilon_n$, and (iii) $\mu_R<\varepsilon_{n-1}<\varepsilon_n<\mu_L$ as shown in Fig. 10(b). In case (i), the fraction of those electrons with the energies $\varepsilon_n\le\varepsilon\le\mu_L$ in the $i=n$ edge channel become transmitted to the right-hand side of the barrier, while those with $\mu_R<\varepsilon<\varepsilon_n$ remain reflected. The electrons in the $i\le n-1$ edge channels remain totally transmitted and the electrons in the $n+1\le i$ edge channels remain perfectly reflected. Here and below, we restrict our consideration to a range of $\Delta\mu<2\hbar\omega_c$ for simplicity. A top view of the transmission and the reflection is schematically shown for the $i=n-1$, n, and $n+1$ edge channels, respectively, in Fig. 9(b). The shadings indicate the regions occupied by electrons. The total transmitted current thereby increases by $(2e/h)(\mu_L-\varepsilon_n)$ to give

$$I=(2e/h)[(n+1)\mu_L-n\mu_R-(n+\tfrac{1}{2})\hbar\omega_c-U_s]\ . \tag{32}$$

By noting the restriction imposed on the values of U_s and by substituting $\mu_{L,R}$ with $\varepsilon_F\pm\Delta\mu/2$, we find that the values of the current are bounded by the interval $(2e/h)[(n+1)\Delta\mu-\hbar\omega_c]\le I\le(2e/h)(n\Delta\mu+\hbar\omega_c)$. If intra-edge-channel scattering is neglected in the barrier region, an inverted population is formed in the $i=n$ edge channel at the UR boundary of the barrier region. In case (ii), the fraction of the electrons in the $i=n-1$ edge channel, which are of energies $\varepsilon\le\varepsilon_{n-1}$, are reflected to cause an inverted population in the $i=n-1$ edge channel, again, at the UR boundary of the barrier region as shown in Fig. 10(b), case (ii). The total transmitted current is given by

$$I=(2e/h)[n\mu_L-(n-1)\mu_R-(n-\tfrac{1}{2})\hbar\omega_c-U_s]\ ,$$

the values of which are bounded by the interval

$$(2e/h)[(n+1)\Delta\mu-2\hbar\omega_c]\le I\le n(2e/h)\Delta\mu\ .$$

In case (iii), inverted population is caused both in the $i=n-1$ and n edge channels at the UR boundary of the barrier region as shown in Fig. 10(b), case (iii), with the total transmitted current

$$I=(2e/h)[(n+1)\mu_L-(n-1)\mu_R-2n\hbar\omega_c-2U_s]\ .$$

The values of the current are in the range

$$n(2e/h)\Delta\mu\le I\le(2e/h)[(n+1)\Delta\mu-\hbar\omega_c]\ .$$

The saddle-point potential U_s determines which one of the above three cases is realized. The current I increases superlinearly with increasing $\Delta\mu$ in cases (i) and (iii),

while it increases sublinearly with $\Delta\mu$ in case (ii). We should note that, in any case, (1) inverted population is expected at the UR boundary of the barrier region, and (2) the difference of the currents carried by the $i=n-1$ and n edge channels (at the LL and UR boundaries) no longer increases linearly with $\Delta\mu$ but is limited to $\Delta I=(2e/h)\hbar\omega_c$; viz., the effective amplitude of the nonequilibrium population introduced in the two edge channels does not exceed $\hbar\omega_c$ as pointed out in Ref. 7. We stress that the above-mentioned features are independent of details of the potential barrier if it is slowly varying. A similar type of population inversion was inferred earlier in a theoretical work of Jain and Kivelson.[38]

Let us turn to our experimental arrangement. We have to predict U_s for a given $\Delta\mu$. As repeatedly emphasized by Landauer[56] and also noted by Büttiker,[57] a profile of the electrostatic potential around a single (ionized) impurity changes with increasing the incident flux of charge carriers on the impurity. In our experiments, a sheet charge induced on the gate electrode by the gate bias voltage is an isolated remote "ionized impurity" for our 2D EG. As shown below, the potential barrier caused by this "ionized impurity" greatly changes with increasing current although the charge and the mechanical location of the "ionized impurity" remains the same. Let us start from such a condition that N Landau levels are completely occupied in the ungated regions while only n Landau levels ($n\leq N-1$) are completely occupied in the gated region *when the current is infinitesimal.* In a clean sample, this condition (N,n) at $I=0$ is realized by the Fermi energy of $\varepsilon_F=N\hbar\omega_c$ and by the electrostatic potential of

$$U(x,y)=0 \quad \text{in the ungated 2D EG regions}$$

and

$$U(x,y)=(N-n)\hbar\omega_c \quad \text{in the gated 2D EG region}$$

except in the boundary regions, as schematically shown in Fig. 11(a) for the case of $(N,n)=(2,1)$. At the sample boundaries, $U(x,y)$ increases to confine the 2D EG, and it varies smoothly at the boundary region between the gated and ungated regions. We will assume also that the current-induced change in $U(x,y)$ is spatially smooth.

We need guiding principles to predict how $U(x,y)$ varies with $\Delta\mu$ or I. Remember that we increase I while keeping the gate bias voltage V_G unchanged with respect to a current contact 1 or 2 in Fig. 2(a). The effective gate bias voltage with respect to the 2D EG underneath the gate thus changes because $U(x,y)$ varies. However, the magnitude of the change is limited to the voltage difference between the two current contacts $\Delta\mu/e$. Since we will study a range of relatively small currents such that $\Delta\mu/e<12$ mV, the effective change is negligibly small compared to the applied V_G, which is typically a few hundreds of mV. Therefore, the electron density beneath the gate is nearly kept unchanged even in the presence of current. It is clear that the electron density in the ungated 2D EG regions should also be kept unchanged. Hence, we have the following guiding principle.

(a) In the presence of current, $U(x,y)$ *adjusts itself so that n bulk Landau states* $(0\leq i\leq n-1)$ *remain completely filled in the* 2D EG *region beneath the gate and N bulk Landau states* $(0\leq i\leq N-1)$ *remain completely filled in the ungated 2D EG regions.*

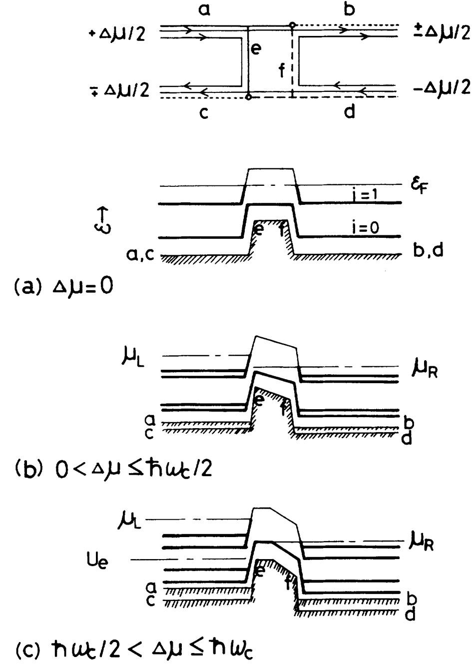

FIG. 11. The drawing on the top shows the current-induced change of the electrochemical potential in the $i=0$ and 1 edge channels when the current is small in the condition of $(N,n)=(2,1)$. (a)–(c) indicate the profiles of the electrostatic potential $U(x,y)$ and of Landau energy levels $\varepsilon_i=(i+\frac{1}{2})\hbar\omega_c+U(x,y)$ along edges a-b and c-d, for three different stages of $\Delta\mu$ smaller than $\hbar\omega_c$. The system is in a linear transport regime for any stages. Heavy lines for Landau levels indicate the occupation with electrons.

The term "electron density" or the "bulk states" in the gated region is of physical meaning because the dimension of our cross gate (1 μm$\times$30 μm) is much larger than the magnetic length and is also probably larger than the screening length of the 2D EG. The requirement (a) has the priority over another requirement (b) introduced below.

When we increase current $I=n(2e/h)\Delta\mu$ in a sufficiently small range, the electrochemical potentials of edge channels will change from ε_F by the amounts $\pm\Delta\mu/2$ as shown on the top of Fig. 11. As the second guiding principle, we assume the following.

(b) Local change in the electrostatic potential $\Delta U(x,y)$ *equals the local change in the electrochemical potential.*

So long as (b) does not contradict (a), this is a reasonable assumption because the capacitance of edge states between different boundaries is extremely small and the chemical part in the electrochemical potential is negligibly small in the present configuration. So, the electrostatic potential increases by $\Delta\mu/2$ at boundaries a and e (solid lines on the top of Fig. 11), and decreases by $\Delta\mu/2$ at boundaries d and f (dashed lines). Here, we focus our attention on the "boundaries of the bulk region,"

a,b,c,d,e, and f, at which $U_a = U_b = U_c = U_d = 0$ and $U_e = U_f = (N-n)\hbar\omega_c$ when $I=0$. Since we assume that $U(x,y)$ smoothly varies, and since the distance between the boundaries of the bulk region defined above and the locations of the relevant edge channels are extremely small compared to the typical size of the sample, we expect that the electrostatic potentials change to $U_{a,d} = \pm\Delta\mu/2$ and $U_{e,f} = (N-n)\hbar\omega_c \pm \Delta\mu/2$ as shown in Fig. 11(b), where + and − signs refer to edge a,e and d,f, respectively. The saddle-point potential corresponding to the barrier height, $U_s = U_e$, thus increases from $(N-n)\hbar\omega_c$ to $(N-n)\hbar\omega_c + \Delta\mu/2$. At boundaries b and c (dotted lines), where the electrochemical potential changes differently for differing edge channels, $U_{b,c}$ change by the value averaged over the edge channels; namely, $U_b = -U_c = [(n/N)-(1/2)]\Delta\mu$. We should note that the potential barrier is flat in the direction across the sample (x direction) while the electrostatic potential in the ungated region has a slope.

The threshold energies, $\varepsilon_i = (i+\frac{1}{2})\hbar\omega_c + U_s$, increase while $\mu_R = N\hbar\omega_c - \Delta\mu/2$ decreases with increasing $\Delta\mu$. Neither of the inequalities (30) and (31) is destroyed until $\Delta\mu = \hbar\omega_c/2$ is reached, at which μ_R equals ε_{n-1}. If the barrier height would continue to increase as $U_s = (N-n)\hbar\omega_c + \Delta\mu/2$ with further increasing $\Delta\mu$, inequality (30) would be violated so that a gated bulk region in the vicinity of boundary e is unoccupied by $i=n-1$ electrons. Since this implies a buildup of positive charges there, the electrostatic potential should drop to such an extent that the gated region is just fully occupied by the $i=n-1$ electrons. This means that the barrier high adjusts itself so that ε_{n-1} equals μ_R, or $U_s = U_e = (N-n+\frac{1}{2})\hbar\omega_c - \Delta\mu/2$. This is required by (a) given above. The profile of the electrostatic potential is shown in Fig. 11(c). The system is still in a linear transport regime.

With increasing $\Delta\mu$ beyond $\hbar\omega_c/2$, the threshold energies ε_i now decrease because U_s decreases, while $\Delta\mu_L = N\hbar\omega_c + \Delta\mu/2$ increases. The system enters the nonlinear regime when $\Delta\mu$ exceeds $\hbar\omega_c$ to make μ_L larger than ε_n. Even in this case, $\mu_R = \varepsilon_{n-1}$ or

$$U_s = (N-n+\tfrac{1}{2})\hbar\omega_c - \Delta\mu/2$$

must be satisfied so that condition (a) is fulfilled. Hence, a nonlinear regime of case (i) with $\mu_R = \varepsilon_{n-1}$ in Fig. 10(b) is introduced in our experiments when $\Delta\mu$ exceeds $\hbar\omega_c$. Substituting in Eq. (32) the value of U_s in the above and $\mu_{L,R} = N\hbar\omega_c \pm \mu/2$, we obtain

$$I = (2e/h)[(n+1)\Delta\mu - \hbar\omega_c] \; . \tag{33}$$

The other cases, (ii) and (iii), in Fig. 10(b) would be met when the gate bias condition is such that the $i=n-1$ bulk Landau level in the region underneath the gate is partially unoccupied. We will not discuss these situations below.

Before comparing Eq. (33) with experiments, let us examine the landscape of $U(x,y)$ to confirm that the requirement (a) can be fulfilled throughout the sample. The profiles of $U(x,y)$ and of Landau levels on cross sections $a-c$ and $b-d$ are schematically shown for the case of $(N,n)=(2,1)$ on the left and on the right of Fig. 12(a). The drawing in the middle of Fig. 12(a) shows similar profiles along boundaries $a-b$ and $c-d$. The heavy lines for Landau levels indicate the occupation by electrons. The landscape of the $i=n$ Landau level and the flow of currents are schematically shown in Fig. 12(b). In this nonlinear regime, U_a and U_d are, similarly to the linear regime, given by $\pm\Delta\mu/2$, but U_c changes to $U_c = \hbar\omega_c/N - [(n+1)/N - \frac{1}{2}]\Delta\mu$ because of the change of the electrochemical potential of the $i=n$ edge channel from μ_L to ε_n at boundary c. The electrostatic potential U_b would be $U_b^* = -U_c$ if all the edge channels were equilibrated. However, if $U_b = U_b^*$, the highest Landau level ($i=N-1$) cannot be filled in a region of U_b^* by the electrons elastically reflected by the barrier because $\mu_R = N\hbar\omega_c - \Delta\mu/2$ is smaller than the energy of the topmost $i=N-1$ Landau level $\varepsilon_{N-1} = (N-\frac{1}{2})\hbar\omega_c + U_b^*$ when $\Delta\mu > \hbar\omega_c$. Hence, from (a), U_b adjusts itself so that the $i=N-1$ Landau level is just completely filled by the reflected electrons in the bulk region; namely, we have $U_b = (\hbar\omega_c - \Delta\mu)/2$ from $\mu_R = \varepsilon_{N-1}(U_b)$. Although not drawn in Fig. 12, equilibration among edge channels is expected to develop as they depart from the potential barrier. Thus, U_b is expected to increase up to U_b^* at a sufficient distance from the barrier, as will be denoted as point $b3$ in Fig. 14. Hence, a "pocket" is expected in the landscape of $U(x,y)$ in the vicinity of the UR corner of the barrier. Note that the electrons in the $i=N-1$ Landau level in such a remote region where $U(x,y) = U_b^*$ are not supplied by the reflection of $i=N-1$ electrons at the barrier but are supplied *via* IES scattering by those electrons transmitted across the barrier along the $i \le n$ edge channels. The consideration in the last half of this paragraph closely relates to a problem addressed by van Son and Klapwijk about an *electron-injecting* current contact.[17]

Equation (33) can be directly examined by experiments. Figure 13 shows the current I as a function of

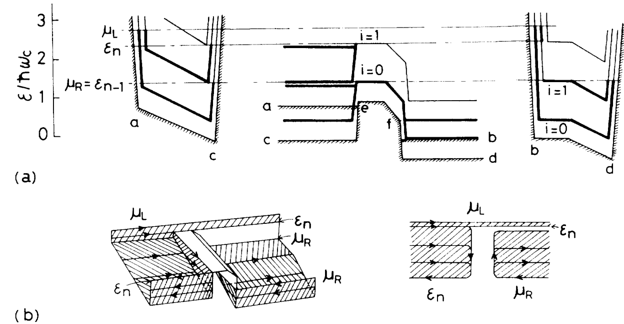

FIG. 12. Schematic representations of the electrostatic potential and Landau levels when $\Delta\mu > \hbar\omega_c$ in the condition of $(N,n)=(2,1)$. (a) The profiles on the cross sections *a-c*, *a-b*, *c-d*, and *b-d*. The heavy lines indicate the occupation of Landau levels with electrons. (b) The landscape of the $i=1$ Landau level with the shaded area indicating the region occupied by electrons, on the left. The top view is on the right.

$\Delta\mu=\mu_L-\mu_R$ for the three sets of conditions $(N,n)=(3,1)$, (3,2), and (2,1). In the experiments, the dc current I is passed from contact 2 to contact 1 and the voltage difference $V_{36}=V_3-V_6=\Delta\mu/e$ between contacts 3 and 6 is measured. This four-terminal resistance is, effectively, a two-terminal resistance of the potential barrier. We have studied opposite polarities of the current and found that the curve of I vs $\Delta\mu$ is perfectly symmetric about $I=0$. This assures our expectation that the change in the gate bias condition with increasing I is negligible. For each set of (N,n), the current I increases linearly with $\Delta\mu=eV_{36}$ following the expected relation $I=n(2e/h)\Delta\mu$ until a critical $\Delta\mu$ is reached to cause superlinear increase in I. The critical $\Delta\mu$ depends on the magnetic field (or N) but not on n, and agrees with $\hbar\omega_c$ as is marked by the arrow in each figure. The agreement of the experimental curve with Eq. (33) in the range $\Delta\mu>\hbar\omega_c$ is excellent for $(N,n)=(3,1)$. For the cases of $(N,n)=(3,2)$ and (2,1), Eq. (33) explains the superlinear increase of I in the range $\Delta\mu>\hbar\omega_c$, but the quantitative agreement is not very excellent. When we derived Eq. (33), we have assumed that the potential U_e at boundary e of the gated 2D EG region equals the potential in the neighboring bulk region underneath the gate. In a narrow boundary region along edge e, however, the potential U_e can be pulled up to a slightly higher level than that of the gated bulk region. Hence, the saddle-point potential $U_s=U_e$ can be slightly higher than the assumed value; viz., $U_s>(N-n+\frac{1}{2})\hbar\omega_c-\Delta\mu/2$ and, hence, $\varepsilon_{n-1}>\mu_R$. Thus, it is possible that the system falls into case (iii). The observed values of the current for $(N,n)=(3,2)$ and (2,1) are bounded by Eq. (33) and $I=n(2e/h)\Delta\mu$, which is expected for case (ii). It is difficult, however, to theoretically derive accurate values of U_s.

We completely ignored random potentials in the sample throughout this subsection. Random potentials of a force range shorter than l_B and of a force range longer than l_B should be considered separately. It is possible to disregard the short-range random potential if we note that it works to broaden each Landau level. The very sharp cyclotron-resonance absorption lines, experimentally observed in high-mobility $GaAs/Al_xGa_{1-x}As$ heterojunctions,[58] indicate that the broadening of Landau levels due to the short-range potential is far smaller than $\hbar\omega_c$. The long-range potentials, on the other hand, modify the equipotential contours along which quasiclassical electron trajectories are developed. What matters in our arguments above is not the absolute landscape of $U(x,y)$ but its change with increasing current. We therefore suppose that the presence of random potentials does not cause essential errors in our picture.

B. Inverted population and energy transport

The most interesting feature of the nonlinear transport described in the last subsection is the formation of inverted population. When the gated area is large in size, the inverted population would relax to some extent through intra-edge-channel scattering at the sample boundary underneath the gate. In any case the excess energy associated with the inverted population is expected to be released at the edge in the vicinity of the UR corner of the gated 2D EG region. Klass *et al.* have recently observed images of energy dissipation in a $GaAs/Al_xGa_{1-x}As$ heterostructure device with a cross gate by using the

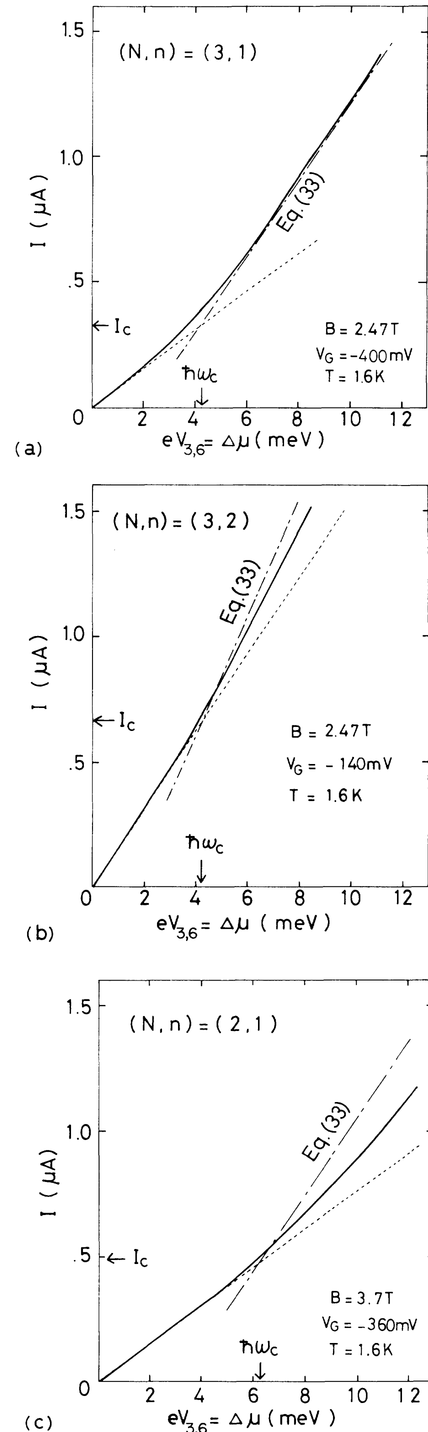

FIG. 13. The current $I=I_{2,1}$ vs voltage $V_{3,6}$ in the conditions of $(N,n)=(3,1)$, (3,2), and (2,1). The dashed line (— — —) indicates the linear relation $I=n(2e/h)\Delta\mu$ and the dash-dotted line (—· —· —·) indicates Eq. (33) for each figure.

fountain-pressure effect of superfluid helium.[36] The size of the gate and the distance between the gate and contacts are typically 100–500 μm. They observed, in the condition of $(N,n)=(3,2)$, four dominant regions of energy dissipation as marked by the circles in Fig. 14(a). They indeed discovered that the energy dissipation is larger at the corner of the gated region where we expect inverted population to take place. They also found that still larger energy is dissipated at the edges of current contacts. To obtain a deeper understanding, let us quantitatively analyze the energy dissipation. The current of 15 μA is applied in the experiment of Klass *et al.*, which corresponds to $\Delta\mu \sim 15\hbar\omega_c$ according to Eq. (33). Although our picture was apparently based on the assumption of $\Delta\mu < 2\hbar\omega_c$, our results also apply without modification to the range of $\Delta\mu > 2\hbar\omega_c$ under the conditions of the experiment of Kla β *et al.* where $N-n=1$: Our picture would have to be modified when treating a case of $N-n \geq 2$, where inverted population forms as well in the edge channels of $i \geq n+1$ when $\Delta\mu > 2\hbar\omega_c$.

Similar to the charge carrier transport, energy transport by carriers can be formulated by a Büttiker-type approach when charge e is replaced with the energy $\varepsilon - \varepsilon_F$ of the electron. Two of us have earlier derived a general formula for the energy transport,[10] which we will use here. On the right-hand side of the gated region of the sample shown in Fig. 14(a), the net energy flux P_b is carried along the edge channels by the fraction of those electrons on side b which are of the energies $\mu_R \leq \varepsilon \leq \mu_L$. It is explicitly written as

$$P_b = (2/h) \sum_{i=0}^{N-1} \int_{\mu_R}^{\mu_L} (\varepsilon - \mu_R) f_i d\varepsilon \ , \qquad (34)$$

where $f_i(\varepsilon)$ is the distribution function of the ith edge

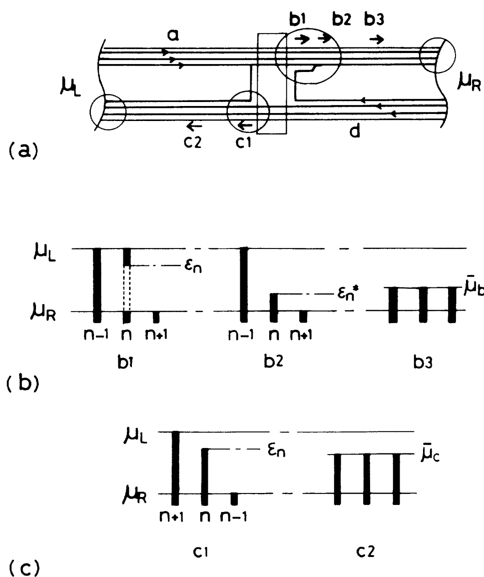

FIG. 14. (a) Four dominant regions of energy dissipation, shown by circles. (b) and (c) Populations in edge channels at different locations.

channel. To evaluate P_b, let us take case (ii) in Fig. 10(b) with $\varepsilon_{n-1} = \mu_R$ as an example. At point $b1$, just at the UR corner of the gated region, where the population is inverted in the $i=n$ edge channel, $f_n(\varepsilon)=1$ for $\varepsilon_n \leq \varepsilon \leq \mu_L$ and $f_n(\varepsilon)=0$ for $\mu_R \leq \varepsilon \leq \varepsilon_n$ as schematically shown on the left-hand side, in Fig. 14(b). Although not considered in Fig. 12, the inverted population will relax through intra-edge-state scattering, and energy is thereby dissipated, probably *via* acoustical-phonon emission. This process may be rapid because the wave functions significantly overlap within a single edge channel. The distribution function thereby changes to give $f_n(\varepsilon)=1$ for $\varepsilon < \varepsilon_n^* = \mu_R + \mu_L - \varepsilon_n$ at point $b2$ as shown in the middle of Fig. 14(b). If IES equilibration length is extremely long as observed in the linear regime, this nonequilibrium distribution will reach the contact on the right. As will be discussed in the following subsections, however, our experiments show that the effective equilibration length is significantly reduced ($\ll 50$ μm) in the nonlinear regime. Hence, IES relaxation follows to achieve the equilibrium population among all the edge channels to give $f_i(\varepsilon)=1$ for

$$\varepsilon < \bar{\mu}_b = [(n+1)\mu_L + (N-n)\mu_R - \varepsilon_n]/N$$

at point $b3$ as shown on the right-hand side of Fig. 14(b). The energy flux is, of course, *different* among the above three stages whereas the transported charge current is the same, being given by Eq. (33). Substituting in Eq. (34) the distribution functions mentioned above together with $\mu_{L,R} = N\hbar\omega_c \pm \Delta\mu/2$ and $\varepsilon_n = (N+1)\hbar\omega_c - \Delta\mu/2$, we immediately derive the respective energy fluxes,

$$P_{b1} = [(n+1)(\Delta\mu)^2 - (\hbar\omega_c)^2]/h \ ,$$

$$P_{b2} = [(n+1)(\Delta\mu)^2 - 2\hbar\omega_c \Delta\mu + (\hbar\omega_c)^2]/h \ ,$$

and

$$P_{b3} = [(n+1)\Delta\mu - \hbar\omega_c]^2/(Nh) \ .$$

The total energy dissipation at the upper right corner of the gated region is

$$P_{\mathrm{UR}} = P_{b1} - P_{b3} \ .$$

The energy dissipated at the upper edge of the right contact is P_{b3}. On the left-hand side to the gated region, where the edge channels on side a are completely filled up to the higher electrochemical potential μ_L, it is convenient to regard the energy flux to be carried by *holes* on side c; namely,

$$P_c = (2/h) \sum_{i=0}^{N-1} \int_{\mu_R}^{\mu_L} (\mu_L - \varepsilon) f_i^h d\varepsilon \ , \qquad (35)$$

where $f_i^h = 1 - f_i(\varepsilon)$ is the hole distribution function in the ith edge channel. The population just at the LL corner of the gated region, as shown by $c1$ in Fig. 14(c), will relax to the equilibrium one shown by $c2$, where $f_i(\varepsilon)=1$ up to

$$\varepsilon = \bar{\mu}_c = [(N-n-1)\mu_L - n\mu_R + \varepsilon_n]/N \ .$$

Noting the symmetry between the electron and hole dis-

tributions, we have $P_{c1}=P_{b2}$ and $P_{c2}=P_{b3}$. Hence, the energy dissipation at the lower left corner of the gated region is

$$P_{\rm LL}=P_{b2}-P_{b3} \ .$$

The rate of energy dissipation in the contact on the left is $P_{c2}=P_{b3}$.

The equations above show that $P_{3b} \gg P_{\rm UR} \gg P_{\rm LL}$ if $\Delta\mu \gg \hbar\omega_c$. For instance, $P_{3b}=645$, $P_{\rm UR}=29$, and $P_{\rm LL}=0.7$ in units of $(\hbar\omega_c)^2/h$ when $(N,n)=(3,2)$ and $\Delta\mu=15\hbar\omega_c$. Our picture thus provides a satisfactory account for the observations by Klass *et al.* It is easy to show that the total energy dissipation in the sample, $2P_{b3}+P_{\rm LL}+P_{\rm UR}$, exactly balances with the electrical power fed into the sample by an external circuit, $P=I(\mu_L-\mu_R)/e$, where I is given by Eq. (33). In the linear regime, the energy dissipation is symmetric around the potential barrier; it is simple to show that $P_{b1}=P_{b2}=P_{c1}=n(\Delta\mu)^2/h$ and $P_{3b}=P_{2c}=(n/N)(\Delta\mu)^2/h$.

C. Rearrangement of edge states and onset of acoustical-phonon emission

There is a series of nonlinear effects which do not influence the two-terminal resistance of a barrier. Even in the range $\Delta\mu<\hbar\omega_c$, where the two-terminal resistance is in the "linear transport regime," those resistances relevant to a voltage probe on the boundary where edge states are unequally populated display *nonlinear* behavior as was first reported in Ref. 7. We have briefly interpreted the effects in Ref. 19. Here, we will discuss the phenomena in detail.

Let us take the two-channel case. A nonequilibrium population is achieved by depleting electrons in one edge channel and accumulating electrons in the other edge channel. The depletion and the accumulation immediately lead to differing chemical potentials, $\Delta\mu^0_{\rm ch}$ and $\Delta^1_{\rm ch}$ of the two edge states. In addition, positive and negative line charges thereby piled up along the edge states modify the original edge potential from $U(x)$ to $U(x)+\Delta U(x)$, which, in turn, changes the edge-state energy dispersion to

$$\varepsilon'_{i,k}(x)\simeq\varepsilon_{i,k}(x)+\Delta U(x) \ ,$$

as schematically shown in Fig. 15(a). Letting x_i and x'_i be the x coordinates at which $\varepsilon_{i,k}(x_i)=\varepsilon_F$ and $\varepsilon'_{i,k}(x'_i)=\mu_i$, respectively, the electrochemical potentials μ_i of the ith edge channels can be expressed as

$$\mu_i=\Delta\mu^i_{\rm ch}+\Delta U(x'_i)+\varepsilon_F \ ,$$

where $\Delta\mu^i_{\rm ch}=\varepsilon_{i,k}(x'_i)-\varepsilon_F$. The difference in the electrochemical potential $\Delta\mu_{01}=\mu_0-\mu_1$ between the edge channels is

$$\Delta\mu_{01}=\Delta\mu_{\rm ch}+\Delta U_{01} \ , \tag{36}$$

where $\Delta\mu_{\rm ch}=\Delta\mu^0_{\rm ch}-\Delta\mu^1_{\rm ch}$ and $\Delta U_{01}=\Delta U(x'_0)-\Delta U(x'_1)$. The pileup charges consist of the electrons and holes located, respectively, in the intervals of $x_0\le x\le x'_0$ and $x'_1\le x\le x_1$. We represent the line charge densities at the respective edge states by Q_0 and Q_1. Let us assume for simplicity that $\Delta x_0=x'_0-x_0$ equals $\Delta x_1=-x'_1+x_1$. Since the number of the states whose center coordinate $x=-l_B^2k$ lies in the interval Δk is generally given by $\Delta k/\pi$ when spin states are degenerated, the line charge densities, Q_0 and Q_1 are of an equal amplitude, $Q=Q_0=-Q_1$, given by

$$Q=e\,\Delta x/(\pi l_B^2) \ , \tag{37}$$

where $\Delta x=\Delta x_0=\Delta x_1$.

Generally, the assumed equality $\Delta x_0=\Delta x_1$ or $Q_0=-Q_1$ is not exact. The sum of the electrochemical potentials, $\mu_0+\mu_1$, is determined by the total current carried by the two edge channels, which is specified by an additional experimental condition. Since Δx_0 and Δx_1 adjust themselves so that both $\Delta\mu_{01}$ and $\mu_0+\mu_1$ meet given experimental conditions, Δx_0 and Δx_1 differ in general. Approximately, the sum of the displacements $\Delta x_0+\Delta x_1$ determines $\Delta\mu_{01}$ while the difference $\Delta x_0-\Delta x_1$ primarily determines $\mu_0+\mu_1$: A finite difference between Δx_0 and Δx_1 leads to a net line charge

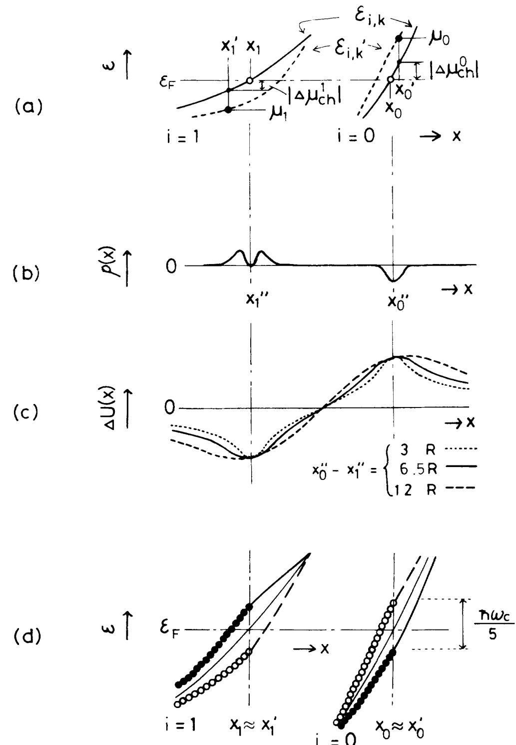

FIG. 15. Rearrangement of edge states due to unequal edge-channel population. (a) A schematic of the original edge states $\varepsilon_{i,k}$ and the modified edge states $\varepsilon'_{i,k}$. (b) A schematic of the pileup charge distribution in the x coordinate. (c) Profiles of the induced electrostatic potential $\Delta U(x)$, calculated according to Eq. (38). (d) Modified edge states, $\varepsilon'_{i,k}=\varepsilon_{i,k}+\Delta U(x)$, for $\Delta\mu=\hbar\omega_c/5$ (dashed lines) and for $\Delta\mu=-\hbar\omega_c/5$ (heavy solid lines), where $x''_0-x''_1=x_0-x_1=6.5R$ and the original dispersions of $\varepsilon_{i,k}$ (light solid lines) are given by Eq. (7) with $\omega_c=9.7\times10^{12}$/s and $\omega_0=1.69\times10^{12}$/ s. Open and solid dots represent the occupation of the states with electrons.

$\bar{Q}=Q_0+Q_1\neq 0$, which substantially determines $\mu_0+\mu_1$ through the electrostatic potentials $\Delta U(x_0')$ and $\Delta U(x_1')$. In a wide sample such as the one used in the present experiments, it is certain that a difference $\Delta x_0-\Delta x_1$ necessary to cause a relatively large change in $\mu_0+\mu_1$, say, by about $\Delta\mu_{01}$, is much smaller that Δx_0 or Δx_1. Hence, Δx_0 and Δx_1 are nearly equal to each other in any experimental condition, and the assumption $\Delta x_0=\Delta x_1$ does not lead to substantial errors in the following discussion.

The line charges have a spatial extent in the x coordinate as well as in the z coordinate (normal to the plane of 2D EG). Let us assume that the charge distribution can be approximated by a uniform distribution of the charge densities $\pm Q/(\pi R^2)$ within the two cylinders of radius R centered at $x_0''=(x_0+x_0')/2$ and $x_1''=(x_1+x_1')/2$. The Poisson equation gives

$$\Delta U(x)=\frac{eQ}{2\epsilon_s}\ln\left|\frac{x-x_1''}{x-x_0''}\right|$$

for $(x_0''+x_1'')/2\le x\le x_0''-R$ and $x_0''+R\le x$, and

$$\Delta U(x)=(eQ/2\epsilon_s)\left[\frac{1}{2}-\frac{1}{2}\left[\frac{x-x_0''}{R}\right]^2+\ln\left|\frac{x-x_1''}{R}\right|\right] \quad \text{for } |x-x_0''|<R \;, \tag{38}$$

where $\epsilon_s=12.8\epsilon_0$ is the dielectric constant of GaAs and $Al_xGa_{1-x}As$. Here, $\Delta U(x)$ is antisymmetric about $x=(x_0''+x_1'')/2$. The relation

$$\Delta U_{01}=\Delta U(x_0')-\Delta U(x_1')\simeq\Delta U(x_0'')-\Delta U(x_1'')$$

immediately yields

$$\Delta U_{01}=(eQ/\epsilon_s)(\tfrac{1}{2}+\ln p)\;, \tag{39}$$

where $p=(x_0''-x_1'')/R$. Note that the separation between the line charges is larger and, hence, ΔU_{01} is larger when the edge potential $U(x)$ is smoother.

The chemical potentials $\Delta\mu_{\rm ch}^i$ in the respective edge channels are given by the relations $Q=\pm eD_i(\varepsilon_F)\Delta\mu_{\rm ch}^i$, where $D_i(\varepsilon_F)=(1/\pi)|\partial\varepsilon_{i,k}/\partial k|_{\varepsilon_F}^{-1}$ are the densities of states of the original edge states at $\varepsilon=\varepsilon_F$. From $\Delta\mu_{\rm ch}=\Delta\mu_{\rm ch}^0-\Delta\mu_{\rm ch}^1$, we have

$$\Delta\mu_{\rm ch}=Q/[eD^*(\varepsilon_F)]\;, \tag{40}$$

where $D^*(\varepsilon)=1/[D_0^{-1}(\varepsilon)+D_1^{-1}(\varepsilon)]$ is the reduced density of states. The densities of edge states $D_i(\varepsilon_F)$ are larger when the edge potential $U(x)$ is smoother. Hence, contrary to ΔU_{01}, $\Delta\mu_{\rm ch}$ is smaller in a smoother edge potential. Noting the relation $\Delta\mu_{01}=\Delta\mu_{\rm ch}+\Delta U_{01}$ with Eqs. (39) and (40), we can rewrite Eqs. (37) and (39) to

$$\Delta x/l_B=\frac{\pi l_B\,\Delta\mu_{01}}{[D^*(\varepsilon_F)]^{-1}+(e^2/\epsilon_s)(\frac{1}{2}+\ln p)} \tag{41}$$

and

$$\Delta U_{01}=\frac{(e^2/\epsilon_s)(\frac{1}{2}+\ln p)\Delta\mu_{01}}{[D^*(\varepsilon_F)]^{-1}+(e^2/\epsilon_s)(1/2+\ln p)}\;. \tag{42}$$

Let us estimate ΔU_{01} and Δx by assuming the edge states determined in Sec. IV (Table I). Let us first estimate the effective radius R of the line charge distribution. Since, as will be shown below, the displacement Δx in the experimental condition is far smaller than the spatial extent of the electron wave function l_B, the real distribution of the pileup charge $\rho(x)$ on the x coordinate is expected to approximately reproduce the profile of the square amplitude of the wave functions; namely,

$$\rho(x)\propto|\phi_{1,k}(x-x_1'')|^2-|\phi_{0,k}(x-x_0'')|^2$$

as schematically shown in Fig. 15(b), where $\phi_{i,k}(x)$ are harmonic-oscillator functions in Eq. (3) with the spatial extent of $l_B=130$ Å. A measure of the width of the charge distribution in the z direction is approximated by $\int_0^\infty z|\zeta(z)|^2dz=3a=105$ Å with the width parameter $a=35$ Å (the Appendix). Hence, we assume the effective radius of the charge distribution to be

$$R=(3al_B/2)^{1/2}=83\ \text{Å}=0.64l_B\;.$$

The approximate spacing between the cylinders is $x_0''-x_1''=r_0l_B=6.5R$. Substituting in Eq. (42) $p=6.5$, $\varepsilon_s=12.8\epsilon_0$, $l_B=130$ Å, and $D(\varepsilon)^*$ with $D_i(\varepsilon)=(1/\pi l_B^2)|\partial\varepsilon_{i,k}/\partial x|^{-1}$, we have $\Delta U_{01}=0.97\,\Delta\mu_{01}$ and $\Delta\mu_{\rm ch}=0.03\,\Delta\mu_{01}$. Thus, the change in the electrostatic potential dominates in our smooth edge potential. Similarly, Eq. (41) derives $\Delta x/l_B=\Delta\mu_{01}/(88.4$ meV). Note that, when $\Delta\mu_{01}$ is not very large, say $\Delta\mu_{01}<2\hbar\omega_c=13$ meV, Δx is far smaller than l_B and is negligibly small compared to the IES spacing $\Delta X_{01}(\varepsilon_F)=r_0l_B$, thus validating the assumptions made in the analysis above. We can approximate both x_i', and x_i'' by x_i in the following discussion.

The solid line in Fig. 15(c) depicts $\Delta U(x)$ as a function of x, where $\Delta U(x)$ is calculated according to Eq. (38) for $p=(x_0-x_1)/R=6.5$. The profile of $\Delta U(x)$ does not crucially depend on the assumed value of R or p, as shown by the dashed and dotted lines in Fig. 15(c). An example of the calculated edge-state energy dispersion $\varepsilon_{i,k}'(x)=\varepsilon_{i,k}(x)+\Delta U(x)$ for the case when $\Delta\mu_{01}=\hbar\omega_c/5=1.2$ meV is shown by the dashed lines and is compared with the original $\varepsilon_{i,k}(x)$ shown by the light solid lines in Fig. 15(d). Open dots represent the occupation by electrons. When $\Delta\mu_{01}$ is negative, the sign of $\Delta U(x)$ is inverted, and we have the energy dispersion represented by heavy solid lines with solid dots indicating the occupation by electrons.

Figure 15(d) indicates that the IES separation, $\Delta X_{01}'(\varepsilon)=X_0'-X_1'$ with $\varepsilon_{i,k}'(X_i')=\mu_i$, for the elastic-scattering process substantially decreases or increases depending on the sign of $\Delta\mu_{01}=\mu_0-\mu_1$. Figure 16(a) shows the separation r'/r_0 as a function of electron energy for the three cases of $\Delta\mu_{01}=0$ and $\Delta\mu_{01}=\pm\hbar\omega_c/5$, where $r'=\Delta X_{01}'(\varepsilon)/l_B$ and $r_0=\Delta X_{01}(\varepsilon_F)/l_B$. The overlapping integral of the wave function, $S'(\varepsilon)=s'(\varepsilon)/s(\varepsilon_F)$, where $s(\varepsilon)'$ is evaluated by replacing r with r' in Eq. (19), changes drastically as shown in Fig. 16(b). The IES scattering, therefore, should be remarkably promoted when $\Delta\mu_{01}$ is positive, and significantly suppressed when

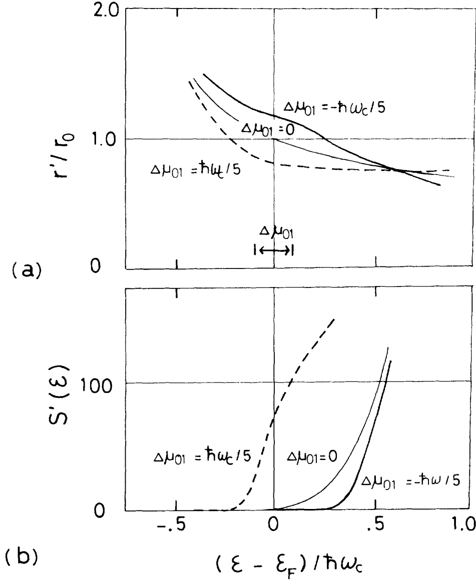

FIG. 16. (a) Modified IES separations r'/r_0. (b) Modified overlapping integrals S'.

$\Delta\mu_{01}$ is negative. Therefore, any resistance should be affected by this effect if at least one of the relevant voltage probes is on the sample boundary at which edge states are unequally occupied. [Note, however, that the two-terminal resistance described in Sec. V A, $R=(\mu_L-\mu_R)/eI$, is unaffected since the total current is unaffected by the IES scattering at one boundary of the sample.]

This effect is demonstrated in Figs. 17(a) and 17(b), where the differential Hall resistances $R'_{m,n}=\partial V_{m,n}/\partial I$ are shown, respectively, for $R'_{3,4}$ and $R'_{5,6}$ as a function of dc bias current I for the case of $(N,n)=(2,1)$. We define I as positive when the electrochemical potential of contact 1 is higher than that of contact 2. $R'_{m,n}$ are obtained by modulating I with a 10-nA amplitude. The resistances display remarkable nonlinear behavior already in the range of current where $\Delta\mu=\mu_L-\mu_R<\hbar\omega_c$: The critical current $I_c=(2e/h)\hbar\omega_c$, at which $\Delta\mu$ equals $\hbar\omega_c$, is marked by solid arrows in the figures. The curves of $R'_{3,4}$ and $R'_{5,6}$ are mutually antisymmetric about $I=0$. The difference in the absolute amplitude between the two resistances is uninteresting here because it arises from different sensitivities of contacts 4 and 5 in selectively probing the $i=0$ and 1 edge channels (parameter α). Theoretically, α can be dependent on I. However, the α of each voltage probe was confirmed to remain unchanged over the I range studied by an additional experiment which observed that the contact resistance[10] of each voltage probe remains unchanged with increasing I. Thus, noting the signs of $\Delta\mu_{01}$ at the diagonally opposite corners of the gated region, we can interpret the observed slopes in the $R'_{m,n}$ vs I curves in a range around $I=0$ as a definite proof of the edge-state rearrangement considered here.[19]

If the IES scattering completely vanished with increasing $|I|$ in the negative $\Delta\mu_{01}$ range, $R'_{3,4}$ and $R'_{5,6}$ should

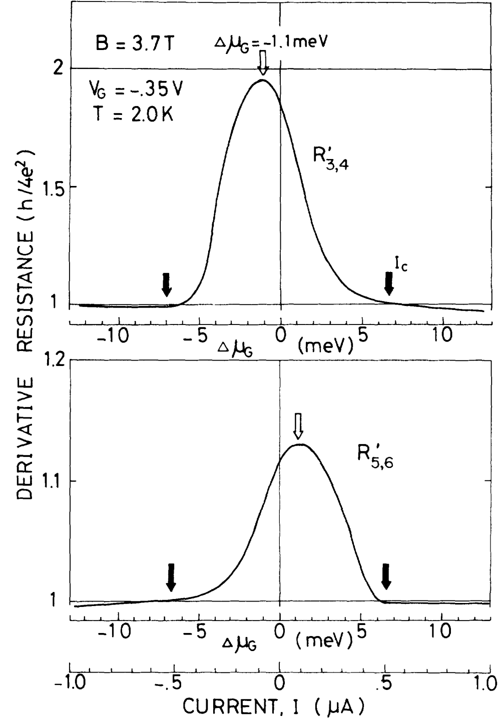

FIG. 17. Differential Hall resistances, $R'_{3,4}=\partial V_{3,4}/\partial I_{1,2}$ and $R'_{5,6}=\partial V_{5,6}/\partial I_{1,2}$, against the dc bias current $I=I_{1,2}$ in the condition of $(N,n)=(2,1)$. The current I is defined to be positive when the electrochemical potential of contact 1 is higher than that of contact 2; hence, $\Delta\mu_{01}$ in the positive range of I is positive for $R'_{3,4}$ and is negative for $R'_{5,6}$.

saturate to the value $R'_{m,n}=(1+\alpha)(h/4e^2)$. However, $R'_{m,n}$ start decreasing rapidly with increasing $|I|$ when $|I|$ exceeds about 0.1 μA. This implies that a new mechanism of IES transition comes to work at $\Delta\mu_{01}\sim 1.2$ meV. This indicates the onset of spontaneous acoustical-phonon emission. Even at $T=0$, phonon emission becomes possible when $\Delta\mu_{01}$ reaches $\hbar c_s q=\hbar c_s r_0/l_B=1.1$ meV, where we note that the relevant IES separation here is $r_0 l_B$ instead of $r_{ac} l_B$. The expected value of $\Delta\mu_{01}$, as marked by open arrows in Figs. 17(a) and 17(b), substantially agrees with the position at which $R'_{m,n}$ start decreasing.[19]

Although the onset of phonon emission is expected as well at the same value of $\Delta\mu_{01}$ in the positive $\Delta\mu_{01}$ range, its influence is not discerned in the $R'_{m,n}$ vs I curves. This is reasonable. When $\Delta\mu_{01}$ approaches 1.1 meV in the positive range, the IES relaxation due to impurity scattering has already been remarkably promoted because of the decreasing $\Delta X'_{01}$. Compared to the impurity scattering, the rate of the $0\rightarrow 1$ transition due to phonon emission is expected to be far smaller because the relevant IES separation is nearly fixed to $\Delta X_{01}(\varepsilon_F)=r_0 l_B$. Returning to the case of $\Delta\mu_{01}<0$, the rate of the $1\rightarrow 0$ phonon emission should be equally low. Nevertheless, this weak transition is practically the single mechanism for the possible IES relaxation when $\Delta\mu_{01}<0$.

The here described asymmetric nonlinear behavior has also recently been observed by Müller *et al.*[20] In Si-

MOSFET's, van Son, Wang, and Klapuijk reported an asymmetric nonlinearity which is of the *opposite* sign.[22] Since the nonequilibrium population of electrons in Si-MOSFET's is caused between the edge states of opposite spins for which the relevant wave functions are significantly overlapped as discussed in Sec. IV B, the nonlinearity cannot be discussed within the framework of our picture here.

D. Saturation of nonequilibrium distribution to $\hbar\omega_c/2$

The differential resistances $R'_{m,n}$ in Fig. 17 nearly reduce to the quantized value $\hbar/4e^2$ in a still higher range of $|I|$. This implies that the deviation of the Hall voltage from the quantized value, $\Delta V_{m,n}=V_{m,n}-(h/4e^2)I$, is saturated to a constant magnitude in the higher-$|I|$ range as pointed out in Ref. 7. The saturation is demonstrated by the direct measurements of $\Delta V_{m,n}$ as shown in Fig. 18(a), where the Hall voltages $V_{m,n}$ are measured as a function of dc current and the quantized Hall voltage $(h/4e^2)I$ is subtracted from $V_{m,n}$. The figure also includes the data of $\Delta V_{6,5}(-B)$ measured in a magnetic field of opposite polarity. In Figs. 18(a) and 18(b), the sign of the current is so chosen as to be identical to the sign of $\Delta\mu_{01}$. We can apply Eqs. (28), (25), and (24) as well as to the regime of nonlinear transport when allowing of possible dependence of α and β on I. Hence, we write

$$\Delta V_{m,n}=\alpha\Delta\mu_V/(2e)=\alpha\beta\Delta\mu_G/(2e)\ , \qquad (43)$$

where $\Delta\mu_V=\mu_{0V}-\mu_{1V}$ represents the unequal population at the entrance of the voltage probe located on the boundary where the nonequilibrium population is introduced. The parameter α of each voltage probe has been confirmed to be kept unchanged with increasing I as noted in the last subsection. Thus, the saturation in ΔV_{mn} should be attributed to the behavior of $\Delta\mu_V$, which is caused by an I dependence either of β or of $\Delta\mu_G$. According to our discussion in Sec. V A, $\Delta\mu_G$ is saturated to $\hbar\omega_c$ to introduce an inverted population when $|I|>I_c=0.5\ \mu$A. However, this does not explain the observed saturation of $\Delta V_{m,n}$ because the complete saturation is established already in a range of $|I|<I_c$.

The size of $\Delta V_{m,n}$ is dependent on the voltage probes, where relevant probes are contacts 4,5, and 6 for $\Delta V_{3,4}$, $\Delta V_{5,6}$ and $\Delta V_{6,5}(-B)$, respectively. The linear relation $I=(2e/h)(\mu_L-\mu_R)$ observed in Fig 13(c) assures that γ of the gate in Eqs. (25)–(28) remains unity in the range $|I|<I_c$, and thus $\Delta\mu_G=\mu_{0G}-\mu_{1G}=(h/2e)I$. Let $\beta_0=\exp(-L/l)$ be the extent of the IES equilibration in the limit of low I. The multiple $\beta_0\alpha$ can be derived from the measurement of $\Delta V_{m,n}=\alpha\beta(h/4e^2)I$ at the limit of small I. Since β_0 lies in the range $0.83\le\beta_0\le 1$ at low temperatures (Sec. IV A), and actually we can suppose $\beta_0\simeq 1$ at the experimental temperature, we can deduce $\Delta\mu_V$ from the observed values of $\Delta V_{m,n}$ through the relation $\Delta\mu_V=2e\ \Delta V_{m,n}/\alpha\simeq 2e\ \Delta V_{m,n}/(\alpha\beta_0)$. All the curves of the so-derived $\Delta\mu_V$ vs I converge to form a single line in the negative $\Delta\mu_G$ range as shown in Fig. 18(c), where the current I is transformed into $\Delta\mu_G=(h/2e)I$. The results here indicate that the saturation in $\Delta V_{m,n}$ is a genuine property of edge states, independent of voltage probes. The values of $\Delta\mu_G$ in Fig. 18(c) are nominal in the range $|\Delta\mu_G|>\hbar\omega_c$ because $|\Delta\mu_G|$ is expected to be saturated to $\hbar\omega_c$. However, they are supposed to be correct within the range $|\Delta\mu_G|<\hbar\omega_c$, on which we will focus our attention below.

To confirm that the phenomena are independent of the difference in the electrochemical potential between the *opposite boundaries* of the sample, we have also studied $\Delta V_{5,6}$ in different gate bias conditions as shown in Fig. 18(b). When the gate bias voltage V_G increases from -0.35 to -0.292 or -0.277 V, partial transmission of electrons takes place in the $i=1$ edge channel so that $\Delta V_{m,n}$ decreases in the linear regime as indicated in Fig. 3. This implies that the parameter γ [Eq. (23)] reduces from unity. The values of γ at $V_G=-0.292$ and -0.277 V can be determined from the two-terminal gate resistance $R_{3,6}=(1/T_G)(h/2e^2)$ in the limit of low current (Fig. 3) through the relation

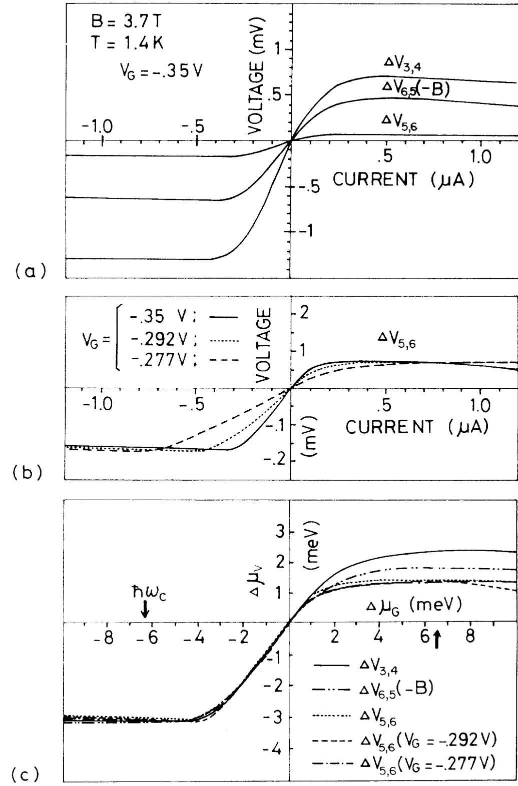

FIG. 18. (a) Deviations of Hall voltages from the quantized value, $\Delta V_{m,n}=V_{m,n}-(h/4e^2)I$, as a function of dc current $I=I_{1,2}$ in the condition of $(N,n)=(2,1)$. Different from Fig. 17, the sign of I is so chosen as to equal the sign of $\Delta\mu_{01}$ for each data. (b) The voltage $\Delta V_{5,6}$ in gate bias conditions of $1\le n<2$. (c) The magnitude of the unequal edge-state population at the entrance of the voltage probe, $\Delta\mu_V=\mu_{0V}-\mu_{1V}$, vs the magnitude of the unequal population produced at the potential barrier, $\Delta\mu_G=\mu_{0G}-\mu_{1G}$.

$$\gamma=[R_{3,6}/(h/4e^2)]-1$$
$$=2/T_G-1=(1-T_{1G})/(1+T_{1G}) .$$

The amplitude of the nonequilibrium population introduced by the gate $\Delta\mu_G=\gamma(h/2e)I$ is now smaller by a factor γ. From a consideration similar to Sec. V A, we expect γ to be kept unchanged with increasing I unless $\Delta\mu_G$ exceeds $\hbar\omega_c=6.4$ meV. The data in Fig. 18(b) show that the position at which the saturation of $\Delta V_{6,5}$ takes place shifts towards larger $|I|$ values with increasing V_G while the saturated value of $\Delta V_{5,6}$ is kept unchanged. When $\Delta V_{5,6}$ at the different V_G's are displayed together against $\Delta\mu_G=\gamma(h/2e)I$, in Fig. 18(c), the curves completely overlap with one another and with the former data in the negative $\Delta\mu_G$ range. We stress that an adjustable parameter is not used to derive any of the data in Fig. 18(c). This demonstrates that only the nonequilibrium population at *one boundary* of the sample is relevant.

Let us focus our attention first on the negative range of $\Delta\mu_G$ in Fig. 18(c), where we have expected in the last subsection only the spontaneous phonon emission to be possible for the IES relaxation in the rage $\Delta\mu_G<-1.1$ meV. The effect of the phonon emission is so small that a resultant structure is hardly discernible in the $\Delta\mu_V$ vs $\Delta\mu_G$ curve. It is important that $\Delta\mu_V$ is saturated to $\Delta\mu_V\simeq=3.2$ meV $=-\hbar\omega_c/2$ already when $\Delta\mu_G$ reaches about -3.2 meV $=-\hbar\omega_c/2$. We conclude from this that an unknown mechanism of very strong IES relaxation becomes effective when $|\Delta\mu_G|$ exceeds $\hbar\omega_c/2$. Let us turn to the positive range of $\Delta\mu_G$, where $\Delta\mu_V$ is saturated as well but the saturated values are smaller, and dependent on particular sample boundaries and/or voltage probes. In the last subsection, w showed that the IES transition due to impurity scattering is much more effective in this positive $\Delta\mu_G$ range. We suppose that the nonequilibrium population of edge states reduces rapidly to $\Delta\mu_{10}=\hbar\omega_c/2$ due to the same unknown mechanism as that for the positive $\Delta\mu_G$ range, and then further equilibrated through impurity scattering. The extent of the impurity-mediated equilibration must be sample-boundary dependent because the concentration of the impurities effective to the IES scattering may be largely dependent on particular boundaries.

We have made similar measurements of $\Delta V_{m,n}=V_{m,n}-[h/(2Ne^2)]I$ in the conditions of $(N,n)=(3,2)$ and (3,1) at $B=2.47$ T ($\hbar\omega_c=4.3$ meV) and observed that $\Delta V_{m,n}$ are again completely saturated when I increases so that $\Delta\mu_G=[h/(2ne)]I$ exceeds $\hbar\omega_c/2$.

We do not have a clear explanation for the saturation mechanism. Would it be possible that our picture of the potential barrier presented in Sec. V A is inadequate and $\Delta\mu_G$ is saturated to $\hbar\omega_c/2$ already at $I=I_c/2$? For this assumption to be consistent with the observed linear increase of I with $\Delta\mu$ in Fig. 13(c), however, the potential barrier has to work in such a way as to partially reflect the $i=0$ edge channel while partially transmitting the $i=1$ edge channel. This appears to the present authors to be very unlikely. It might be useful to give tentative suggestion about possible mechanisms. The edge states might become unstable due to pileup charges when the edge-state rearrangement is so pronounced that the dispersion becomes flat at the edges; $\partial\varepsilon'_{i,k}/\partial x=0$ at $x=x'_i$ in Fig. 15(a). Secondly, a new type of edge-state excitation might be possible, in which electrochemical potentials $\mu_i(y,t)$ of two edge channels oscillate in time and space with opposite phase; namely

$$\mu_0-\varepsilon_F=-(\mu_1-\varepsilon_F)\propto\exp[i(qy+\omega t)] .$$

Such an "optical-mode"-type excitation differs from the known "acoustic-mode" edge magnetoplasma excitations,[59,60] for which different edge states are assumed to be in phase:

$$\mu_0-\varepsilon_F=\mu_1-\varepsilon_F\propto\exp[i(qy+\omega t)] .$$

The "optic-mode" edge magnetoplasma excitations will promote IES scattering at the location where $\Delta\mu_{01}$ takes on the maximum ($qy+\omega t=2n\pi$).

VI. CONCLUSION

The transport properties of a high-mobility 2D EG at strong magnetic fields have been studied in the presence of nonequilibrium population of electrons among edge channels, by using $GaAs/Al_xGa_{1-x}As$ heterostructure devices with a cross gate. Temperature dependence and current-magnitude dependence have both been investigated in detail.

The observed temperature dependence of IES equilibration length studied in the two-channel case is well explained by a quantitative analysis of the IES transition, which explicitly considers a Fermi distribution function in edge states and takes account of a long-range impurity scattering and the acoustical deformation-potential scattering. The observed temperature dependence is consistent with a smooth parabolic confining potential [$U(x)=(m^*/2)\omega_0^2x^2$ for $x>0$ and $U(x)=0$ for $x<0$] with $\omega_0=1.7\times10^{12}$/s, which is also in accord with earlier experiments.[46] The analysis also shows that the impurity potential of a force range of about 160 Å dominates the IES electron transition in the T range studied (1.4–13 K).

Analysis of nonlinear transport across a potential barrier in the quantum Hall regime predicts an inverted population in an edge channel when the electrochemical potential differs by more than $\hbar\omega_c$ across the barrier. The analysis provides a reasonable account of the experimentally observed current dependence of the two-terminal resistance of the barrier. The energy transport by charge carriers has been quantitatively described to show that the here predicted inverted population gives an account for the asymmetric energy dissipation around the potential barrier.

Unequally populated edge states reorganize themselves because the pileup charges along the edge channel significantly modify the electrostatic potential. The rearrangement of edge states leads to a characteristic dependence of the IES equilibration length on the current. This gives rise to an asymmetric nonlinear behavior of those resistances that are relevant to the boundary of a sample at which edge channels are unequally occupied.

This work observed this effect in a Hall resistance. The onset of spontaneous phonon emission promotes the IES equilibration when the amplitude of unequal occupation between relevant edge channels exceeds the threshold value $\Delta\mu=\hbar c_s q=\hbar c_s \Delta X/l_B^2$, where ΔX is the IES separation. This effect is small in absolute magnitude, but causes a distinct structure in a differential resistance.

It was experimentally found that the maximum amplitude to which adjacent edge channels can be unequally populated is limited to $\Delta\mu=\hbar\omega_c/2$, which suggests the onset of an unknown mechanism that efficiently mixes edge states when $\Delta\mu>\hbar\omega_c/2$. The understanding of the mechanism is left for future studies.

ACKNOWLEDGMENTS

One of the authors (S.K.) thanks Dr. L. I. Glazman for suggesting the importance of including the Fermi distribution function into the analysis of the T dependent IES scattering. This work is supported in part by the Industry-University Joint Research Project "Mesoscopic Electronics." This work is also supported in part by the Grants-in-Aid for Scientific Research (B) and for Scientific Research on Priority Area, "Electron Wave Interference Effects in Mesoscopic Structures" both from the Ministry of Education, Science and Culture.

APPENDIX

Squared matrix elements for the inter-Landau-level transition $|0,k_0\rangle\rightarrow|1,k_1\rangle$ due to emission or absorption of an acoustical phonon of wave vector $\mathbf{q}=(q_x,q_y,q_z)$ in the ideal system of bulk Landau levels are given by[45]

$$|\langle 1,k_1|H_{\rm ac}|0,k_0\rangle|^2 =(\hbar E_d^2 q/2\rho V c_s)|\langle 1,k_1|e^{-i\mathbf{q}\cdot\mathbf{r}}|0,k_0\rangle|^2 , \quad \text{(A1)}$$

where $q=|\mathbf{q}|$ and

$$|\langle 1,k_1|e^{-\mathbf{q}\cdot\mathbf{r}}|0,k_0\rangle|^2 =G(q_z)J(q_x,q_y)\delta_{q_y,k_1-k_0}(n_{\rm ac}+\tfrac{1}{2}\pm\tfrac{1}{2}) .$$

Here, δ_{q_y,k_1-k_0} resents the momentum conservation,

$$n_{\rm ac}=[\exp(\hbar c_s q/kT)-1]^{-1}$$

is the phonon occupation number, $\pm$ signs refer to emission and absorption processes, respectively, and

$$G(q_z)=[1+(q_z a)^2]^{-3} ,$$

$$J(q_x,q_y)=(b^2/2)\exp(-b^2/2)$$

with $b^2=(q_x^2+q_y^2)l_B^2$ are obtained by assuming, for $\zeta(z)$ in Eq. (3), the Fang-Howard wave function[61]

$$\zeta(z)=(2a^3)^{-1/2}z\exp(-z/2a) ,$$

with the width parameter

$$a=[12m^*e^2(\tfrac{11}{32}n_s+n_{\rm depl})/(\epsilon_s\hbar^2)]^{-1/3} .$$

A measure of the "thickness" of the 2D EG in the z direction is given by $\int_0^\infty z|\zeta|^2dz=3a$. For our 2D EG, $a=35$ Å is obtained with the 2D EG density $n_s=3.4\times10^{11}/\text{cm}^2$, the depletion charge density $n_{\rm depl}=5\times10^{10}/\text{cm}^2$, and the dielectric constant $\epsilon_s=12.8\epsilon_0$ of GaAs.

Since the wave functions $\phi_{i,k}(x-X_i)$ for our edge states are the harmonic-oscillator functions, the results given above for bulk Landau levels can be used for the edge states with a simplification given below. Noting that $G(q_z)$ and $J(q_x,q_y)$ are, respectively, rapidly decreasing functions of q_z and q_x, and that $\int_{-\infty}^{\infty}G(q_z)dq_z=3\pi/(8a)$ and

$$\int_{-\infty}^{\infty}\exp[-(q_x l_B)^2/2]dq_x=\sqrt{2\pi}/l_B ,$$

we approximate the functions as $G(q_z)=1$ for $|q_z|<(3\pi/16)(1/a)$ and $G(q_z)=0$ otherwise, and

$$J(q_x,q_y)=[(q_y l_B)^2/2]\exp[-(q_y l_B)^2/2]$$

for $|q_x|<\sqrt{\pi/2}(1/l_B)$ and $J(q_x,q_y)=0$ otherwise. For simplicity, we also replace q in Eq. (A1) with q_y, because $q_y=\Delta X_{01}^{\rm ac}/l_B^2\gg 1/l_B$ is much larger than those q_z or q_x for which G and J are nonzero. With these approximations, Eq. (A1) is transformed to Eq. (10) in the text, where $q_y l_B=r_{\rm ac}$.

[1]B. I. Halperin, Phys. Rev. B **25**, 2185 (1982).
[2]A. H. MacDonald and P. Streda, Phys. Rev. B **29**, 1616 (1984).
[3]Y. Ono, T. Ohtsuki, and B. Kramer, J. Phys. Soc. Jpn. **58**, 1705 (1989).
[4]H. Hirai, S. Komiyama, S. Hiyamizu, and S. Sasa, *Proceedings of the 19th International Conference on the Physics of Semiconductors, Warsaw, 1988*, edited by W. Zawadzki (Institute of Physics, Polish Academy of Sciences, Warsaw, 1988), p. 55.
[5]R. J. Haug, A. H. MacDonald, P. Streda, and K. von Klitzing, Phys. Rev. Lett. **61**, 2797 (1988).
[6]S. Washburn, A. B. Fowler, H. Schmid, and D. Kern, Phys. Rev. Lett. **61**, 2801 (1988).
[7]S. Komiyama, H. Hirai, S. Sasa, and S. Hiyamizu, Phys. Rev. B **40**, 12 566 (1989).
[8]B. J. van Wees, E. M. M. Willems, C. J. P. M. Haarmans, C. W. J. Beenakker, H. van Houten, J. G. Wiiliamson, C. T. Foxon, and J. J. Harris, Phys. Rev. Lett. **62**, 1981 (1989).
[9]M. Büttiker, Phys. Rev. B **38**, 9375 (1988).
[10]S. Komiyama and H. Hirai, Phys. Rev. B **40**, 7767 (1989).
[11]S. Komiyama, H. Hirai, S. Sasa, and T. Fujii, Solid State Commun. **73**, 91 (1990).
[12]H. Hirai, S. Komiyama, S. Sasa, and T. Fujii, J. Phys. Soc. Jpn. **58**, 4086 (1989).
[13]B. W. Alphenaar, P. L. McEuen, R. G. Wheeler, and R. N. Sacks, Phys. Rev. Lett. **64**, 677 (1990).
[14]G. Müller, D. Weiss, S. Koch, K. von Klitzing, N. Nickel, W. Schlapp, and R. Losch, Phys. Rev. B **40**, 7633 (1990).
[15]S. Komiyama, H. Hirai, S. Sasa, and T. Fujii, Surf. Sci. **229**, 224 (1990).
[16]H. Hirai and S. Komiyama, J. Appl. Phys. **68**, 665 (1990).

[17]P. C. van Son and T. M. Klapwijk, Europhys. Lett. **12**, 429 (1990).

[18]G. Müller, D. Weiss, S. Koch, K. von Klitzing, H. Nickel, W. Schlapp, and R. Lösch, in *Proceedings of the 20th International Conference on the Physics of Semiconductors, Thessaloniki, 1990,* edited by E. M. Anastassakis and J. D. Joannopoulos (World Scientific, Singapore, 1990), p. 829.

[19]S. Komiyama, H. Hirai, M. Ohsawa, H. Matsuda, S. Sasa, and T. Fujii, in *Proceedings of the 20th International Conference on the Physics of Semiconductors, Thessaloniki, 1990,* edited by E. M. Anastassakis and J. D. Joannopoulos (World Scientific, Singapore, 1990), p. 1150.

[20]G. Müller, E. Diessel, D. Weiss, K. von Klitzing, K. Ploog, H. Nickel, W. Schlapp, and R. Lösch, *Proceedings of the 9th International Conference on Electronic Properties of Two-Dimensional Systems, Nara, 1991* [Surf. Sci. (to be published)].

[21]L. W. Molenkamp, M. J. P. Brugmens, H. van Houten, C. W. J. Beenakker, and C. T. Foxon, Phys. Rev. B **43**, 12 118 (1991).

[22]P. C. van Son, S. L. Wang, and T. M. Klapuijk, *Proceedings of the 9th International Conference on Electronic Properties of Two-Dimensional Systems, Nara, 1991* [Surf. Sci. (to be published)].

[23]B. W. Alphenaar, P. L. McEuen, R. G. Wheeler, and R. N. Sacks (unpublished).

[24]B. J. van Wees, E. M. M. Willems, L. P. Kouwenhoven, C. J. P. M. Harmans, J. G. Williamson, C. T. Foxon, and J. J. Harris, Phys. Rev. B **39**, 8060 (1989).

[25]R. J. Haug and K. von Klitzing, Europhys. Lett. **10**, 489 (1989).

[26]P. L. McEuen, S. Szafer, C. A. Richter, B. W. Alphenaar, J. K. Jain, A. D. Stone, R. G. Wheeler, and R. N. Sacks, Phys. Rev. Lett. **64**, 2062 (1990).

[27]P. C. van Son, F. W. de Vries, and T. M. Klapwijk, Phys. Rev. B **43**, 6764 (1991).

[28]J. Faist, Europhys. Lett. **15**, 331 (1991).

[29]C. A. Richter, R. G. Wheeler, and R. N. Sacks, *Proceedings of the 9th International Conference on Electronic Properties of Two-Dimensional Systems, Nara, 1991* [Surf. Sci. (to be published)].

[30]H. Nii, M. Ohsawa, S. Komiyama, S. Fukatsu, Y. Shiraki, R. Itoh, and H. Toyoshima, *Proceedings of the 9th International Conference on Electronic Properties of Two-Dimensional Systems, Nara, 1991* [Surf. Sci. (to be published)].

[31]S. Komiyama, H. Nii, M. Ohsawa, S. Fukatsu, Y. Shiraki, R. Itoh, and H. Toyoshima, Solid State Commun. **80**, 157 (1991).

[32]T. Martin and S. Fend, Phys. Rev. Lett. **64**, 1971 (1990).

[33]J. J. Palacios and C. Tejedo (unpublished).

[34]S. M. Badalian, Y. B. Levinson, and D. L. Maslov, Pis'ma Zh. Eksp. Teor. Fiz. **53**, 595 (1991) [JEPT Lett. **53**, 619 (1991)].

[35]A. V. Khaetskii and K. A. Matveev (unpublished).

[36]V. Klass, W. Dietsche, K. von Klitzing, and K. Ploog, *Proceedings of the 9th International Conference on Electronic Properties of Two-Dimensional Systems, Nara, 1991* [Surf. Sci. (to be published)].

[37]P. Streda, J. Kucera, and A. H. MacDonald, Phys. Rev. Lett. **59**, 1973 (1987).

[38]J. K. Jain and S. A. Kivelson, Phys. Rev. B **37**, 4276 (1988).

[39]T. Ohtsuki and Y. Ono, J. Phys. Soc. Jpn. **58**, 3863 (1989).

[40]L. Smrcka, H. Havlova, and A. Ishihara, J. Phys. C **12**, L457 (1986).

[41]K. F. Berggren, T. J. Thornton, D. J. Newson, and M. Pepper, Phys. Rev. Lett. **57**, 1769 (1986).

[42]W. Walukiewicz, H. E. Ruda, J. Lagwski, and H. C. Gatos, Phys. Rev. B **29**, 4818 (1984).

[43]B. J. F. Lin, D. C. Tsui, M. A. Paalanen, and A. C. Gossard, Appl. Phys. Lett. **45**, 695 (1984).

[44]W. Walukiewicz, Phys. Rev. B **37**, 8530 (1988).

[45]G. A. Toombs, F. W. Sheard, D. Neilson, and L. J. Challis, Solid State Commun. **64**, 577 (1987).

[46]K. F. Berggren, G. Roos, and H. van Houten, Phys. Rev. B **37**, 10 118 (1988).

[47]P. L. McEuen, E. B. Foxman, U. Meirav, M. A. Kastner, Y. Meir, N. S. Wingreen, and S. J. Wind, Phys. Rev. Lett. **66**, 1926 (1991).

[48]A. A. M. Staring, J. g. Williamson, H. van Houten, C. W. J. Beenakker, L. P. Kouvenhoven, and C. T. Foxon, *Proceedings of the 9th International Conference on Electronic Properties of Two-Dimensional Systems, Nara, 1991* [Surf. Sci. (to be published)]; also in *Proceedings of International Symposium on Analogies in Optics and Micro-Electronics, Eindhoven, 1991,* edited by W. van Haerinern and D. Lenstra (North-Holland, Amsterdam, 1991).

[49]H. Hirai, S. Komiyama, K. Nakamura, and H. Nihei, J. Appl. Phys. (to be published).

[50]G. Ebert, K. von Klitzing, K. Ploog, and G. Weimann, J. Phys. C **16**, 5441 (1983).

[51]M. E. Cage, R. F. Dziuba, B. F. Field, E. R. Williams, S. M. Girvin, A. C. Gossard, D. C. Tsui, and R. J. Wagern, Phys. Rev. Lett. **51**, 1374 (1983).

[52]S. Komiyama, T. Takamasu, S. Hiyamizu, and S. Sasa, Solid State Commun. **54**, 479 (1985).

[53]T. Takamasu, S. Komiyama, S. Hiyamizu, and S. Sasa, Surf. Sci. **10**, 202 (1986).

[54]P. Streda, J. Phys. C **19**, L155 (1986).

[55]M. Büttiker, Phys. Rev. B **41**, 7906 (1990).

[56]R. Landauer, IBM J. Res. Develop. **1**, 223 (1957); **32**, 306 (1988).

[57]M. Büttiker, IBM J. Res. Develop. **32**, 317 (1988).

[58]See, for example, M. Besson, E. Gornik, G. Böhn, and G. Weimann, *Proceedings of the 9th International Conference on Electronic Properties of Two-Dimensional Systems, Nara, 1991* [Surf. Sci. (to be published)].

[59]V. A. Volkov and S. A. Mikhailov, Zh. Eksp. Teor. Fiz. **94**, 217 (1988) [Sov. Phys. JETP **67**, 1639 (1988)].

[60]M. Wassermeier, J. Oshinowo, J. P. Kotthaus, A. H. MacDonald, C. T. Foxon, and J. J. Harris, Phys. Rev. B **41**, 10 287 (1990).

[61]F. F. Fang and W. E. Howard, Phys. Rev. Lett. **16**, 797 (1966).